Surface Tension Measurement of
High Density Polyethylene and Its Clay Nanocomposites
in Supercritical Nitrogen

by

Hua Wei

A thesis

presented to the University of Waterloo

in fulfillment of the

thesis requirement for the degree of

Master of Applied Science

in

Chemical Engineering

Waterloo, Ontario, Canada, 2009

AUTHOR'S DECLARATION

I hereby declare that I am the sole author of this thesis. This is a true copy of the thesis, including any required final revisions, as accepted by my examiners.

I understand that my thesis may be made electronically available to the public.

Hua Wei

Abstract

Surface tension of a polymer melt in a supercritical fluid is a principal factor in determining cell nucleation and growth in polymer microcellular foaming.

Previous work has presented the surface tension of the amorphous polymer, polystyrene (PS), in supercritical CO_2 determined by Axisymmetric Drop Shape Analysis-Profile (ADSA-P), together with theoretical calculations for a corresponding system. The dependences of the surface tension on temperature, pressure and polymer molecular weight were discussed and the physical mechanisms for three main experimental trends were explained using Self Consistent Field Theory (SCFT).

This thesis introduces recent work on the surface tension measurement of the crystalline polymer, high density polyethylene (HDPE), in supercritical N_2 under various temperatures and pressures. The surface tension was determined by ADSA-P and the results were compared with those of the amorphous polymer PS. The dependence of the surface tension on temperature and pressure, at temperatures above the HDPE melting point, ~125°C, was found to be similar to that of PS; that is, the surface tension decreased with increasing temperature and pressure. Below 125°C and above 100°C, HDPE underwent a process of crystallization, where the surface tension dependence on temperature was different from that above the melting point, i.e., decreased with decreasing temperature. Differential Scanning Calorimetry (DSC) characterization of the polymer was carried out to reveal the process of HDPE crystallization and relate this to the surface tension behavior. It was found that the amount of the decrease in surface tension was related to the rate of temperature change and

hence the extent of polymer crystallization.

In the second part of the thesis, surface tension dependences on temperature, pressure and clay concentrations were studied for HDPE nano-clay composites (HNC) and compared with pure HDPE. It was found the trends with temperature and pressure were the same with PS in CO_2 and HDPE in N_2; that is, the surface tension decreased with increasing temperature and pressure. In all nanocomposite samples, the surface tension decreased compared with pure HDPE. This could be a good explanation for the better polymer foaming quality with the addition of clay in the polymer. A minimum surface tension was found with the sample at ~3% concentration of clay. The degree of crystallinity of HNC was analyzed by Differential Scanning Calorimetry (DSC) at different clay concentrations. A minimum crystallinity was also found at the clay concentration of 3%. The possible relationship between surface tension and polymer crystallinity was discussed.

Acknowledgements

During the past two years, my supervisor Dr. Pu Chen offered me invaluable guidance and opportunities, so first of all, I would like to sincerely thank him.

I also appreciate all of my cosupervisors, Dr. R.B. Thompson in the Department of Physics and Astronomy and Dr. Chul B. Park in Microcellular Plastics Manufacturing Laboratory of University of Toronto for their endless help and advice.

All of the former and current group members, especially Dr. Yuebiao Sheng, Abdolhamid Firooz, Dr. Hyuk Sang Park, Dr. Nasim Hyder, Zhenyu Qian, Hui Wang, Parisa Sadatmousavi and Nancy Wang inspired me a lot in my research. I want to greatly thank all of them for sharing. I would like to thank my friend and proof reader Karishma Irani for her great help.

I would also like to acknowledge Research in Motion for the use of equipment and Dr. Bev Christian for advice and suggestions for many aspects of the research.

Last but not least, I deeply appreciate my parents and friends for their love and supports as always.

Table of Contents

Chapter 4 Surface Tension of High Density Polyethylene in Supercritical Nitrogen

Chapter 5 Surface Tension of High Density Polyethylene-Clay Nanocomposites in Supercritical Nitrogen

List of Figures

List of Tables

Nomenclature

$N_{\text{hom}o}^{0}$ number of nuclei generated per cm^3 per second

C_0 concentration of gas molecules (number of molecules per cm^3)

f_0 frequency factor of the gas molecules

$\Delta G_{\text{hom}o}$ Gibbs free energy for homogeneous nucleation

k_B Boltzmann's constant

ΔP pressure difference across the polymer-gas interface

R1   Radius of curvature in the plane of paper, cm

R2   Radius of curvature in a plane perpendicular to paper, cm

γ interfacial tension

ΔP_0 pressure difference at a reference datum plane

$\Delta \rho$ the difference in the density of the two bulk phases

G   gravitational acceleration

z vertical height measured from the reference plane.

s   arc length measured from the origin

θ_e contact angle

γ_{sv} solid-gas interface

γ_{lv},   gas-liquid interface

γ_{sl} liquid-solid interface

W_{tot} total weight

W_{ring} weight of the ring

M	molecular weight
$\gamma(\infty)$	surface tension for infinite molecular weight
T	temperature, ℃
P	pressure, psi
v_p	specific volume (cm^3/g)
$\tilde{\rho}$	reduced density
$\tilde{P}$	reduced pressure
$\tilde{T}$	reduced temperature
r	number of sites occupied by a molecule
y	occupied lattice site fraction
s	number of segments dividing a molecule
c	volume-dependent degrees of freedom
B_0	Bond number

Chapter 1

Introduction and objectives

1.1 Introduction

Surface tension of polymers is one of the most important physicochemical parameters in lots of polymer engineering processes, such as microcellular foaming in supercritical fluids where the surface tension between the polymer melt and the supercritical fluid is a principal factor in determining cell nucleation and growth (Myers D., 1991). Generally, low surface tension is desired in the polymer foaming process to increase the nucleation rate and produce small and uniform cells (Nishioka *et al.*, 1992). Among all the the methods of measuring surface tension, the pendant drop method is commonly used for polymers, liquid crystals, and other low-molar-mass liquids. (del Rio *et al.*, 1997; Lahooti *et al.*, 1996)

Although the theory of pendant drop method is quite simple , experimental determination of the surface tension of a high viscosity polymer has been very difficult, because of the handling of highly viscous polymer melts at high temperatures and pressures. (Demarquette, *et al.*, 1994; Roe *et al.*, 1967; Wu, 1970; Wu, 1982; Morita *et al.*, 2002 ; Xue *et al.*, 2004)

The Axisymmetric Drop Shape Analysis (ADSA) approach relies on a numerical integration of the Laplace equation of capillarity to quantify the surface tension. This numerical procedure applies to both sessile and pendant drops in shape analysis methods. (Cheng, P. *et al.*, 1990; Susnar, *et al.*, 1994 ; Cheng, P. *et al.*, 1992) Recently, ADSA has been used for determining polymer melt surface tension in supercritical fluids at high temperature and high pressure, (Li, H. *et al.*, 2004) e.g., the surface tension measurement of the amorphous polymer, polystyrene (PS), in supercritical CO_2. (Park, H. *et al.*, 2006; Park,

H. *et al*., 2007)

Surface tension of polymers in supercritical fluids varies with many parameters, e.g., temperature, pressure, and solubility of supercritical fluids. Recent reports (Park, H. *et al*., 2006; Park, H. *et al*., 2007) showed several trends of the surface tension change with temperature and pressure for PS in supercritical CO_2. In general, the surface tension decreases with increasing temperature and pressure. Self-consistent field theory (SCFT) calculations were used to explain these experimental trends. (Park, H. *et al*., 2007)

The degree of crystallinity of a polymer can have a large impact on polymer properties. It is known that polystyrene (PS) is a typical amorphous polymer, and high density polyethylene (HDPE) is a typical crystalline polymer. Both types of polymers are often used in polymer microcellular foaming processes. In molten phase, crystalline polymers and amorphous polymers may behave similarly. This is not the case in the solid state. When the temperature decreases below the melting point, amorphous polymers change into complete solids with disordered chain arrangements, but crystalline polymers would experience the process of crystallization: before a crystalline polymer becomes completely solid, it enters a viscoelastic state, where micro-crystals form and grow into regions of ordered chain arrangements within a continuous polymer melt. And how much crystals are formed and how much degree of crystallinity is generated is based on the rate of the cooling. Surface tension measurement of polymers undergoing such transitions can help clarify the different behavior between amorphous and crystalline polymers. (Wunderlich, 1958) It has been found that the surface tension of amorphous polymers at temperatures below the melting point does not change significantly. But to date, no measurement on the surface tension of

crystalline polymers has been made at temperatures below the melting point. It is plausible that the surface tension of a crystalline polymer may behave differently from that of an amorphous polymer, i.e., the crystalline polymer may respond to variations of temperature below the melting point. A follow up question would then be how temperature, or the rate of temperature change, affects the surface tension, as well as polymer crystallization. (Jürgen and E.K. Schawe, 2007; Wunderlich, 1973; Wunderlich, 1980; Zachmann and H.G. Fortschr., 1964; Pijpers et al., 2002)

 Recently research on the batch foaming process of HDPE-clay nanocomposites (HNC) using supercritical fluids has been conducted. It has been proved that in comparison with pure HDPE, nanocomposites produce much finer and more uniform cell structures. (Y. H. Lee et al., 2005; Y. H. Lee et al., 2007) Till now, no fundamental studies on the surface tension of these nanocomposites in supercritical fluids have been performed. The second part of this work focuses on the surface tension measurement of HDPE-clay nanocomposites in supercritical N_2. The results of HNC with different concentrations of clay are compared with the result of pure HDPE. Then, how the surface tension as well as the polymer crystallinity change with the change of clay concentration will be investigated. This study will have diverse impacts on the process optimizations of microcellular foaming process, which gives an explanation to the better foaming quality of HNC.

1.2 Research Objectives

The primary purpose of this work is to establish an ADSA-based approach for evaluating the surface tension of the crystalline polymer high density polyethylene (HDPE) and its clay

nanocomposites (HNC) in supercritical nitrogen over a wide range of temperatures and pressures. The relationships of surface tension, solubility and crystallization with temperature and pressure will be investigated. The surface tension results of pure HDPE will be compared with those of the amorphous polymer polystyrene, to show the difference between crystalline and amorphous polymers as well as the relationship with fluid solubility. The surface tension of HNC at different clay concentrations will be measured and compared with corresponding polymer crystallinity to find a possible relationship and the minimum point. This study will have diverse impacts on the process optimizations of microcellular foaming process, which includes the understanding of cell nucleation and growth.

This thesis consists of six Chapters: Chapter 1 gives a brief instruction and the research objectives. Chapter 2 contains the literature review regarding recent work on the surface tension measurement of PS in supercritical CO_2, polymer foaming, polymer cystallinity, and HDPE-clay nanocomposites. Chapter 3 describes the experimental approaches. Chapter 4 focuses on a study of surface tension measurement of HDPE in supercritical N_2. Chapter 5 discusses the surface tension of HDPE-clay nanocomposites and its relation with different clay concentration as well as polymer crystallinity. Chapter 6 presents the conclusions and gives recommendations for future work.

Chapter 2

Literature Review

2.1 Polymer Melts in Supercritical Fluids

Plastics are widely used as manufacturing materials all around the world. Particularly, plastic foaming products, with high cell density and uniform cell sizes, offer superior mechanical and improved thermal insulation properties comparing with solid plastic products. Applications of foamed plastics range from daily commodities such as packaging materials, to advanced manufacturing products such as airplane and automotive parts with high strength-to-weight ratio. Further more, plastic foaming products reduce material usage, which typically reach to 50 to 70% of total production cost. In general, all foaming processes involve four main steps as shown in Figure 1: dissolution of gas into a polymer matrix; cell nucleation; cell growth and stabilization of foam structures. (Seeler *et al.*, 1992)
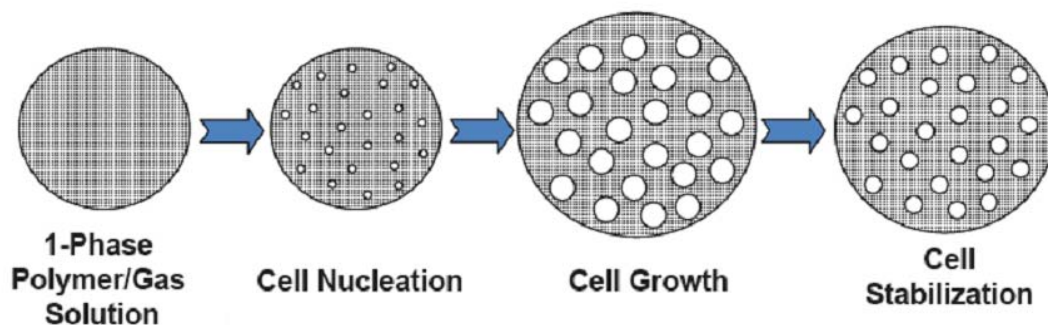
Fig. 1 Main steps of polymer foaming processes

A supercritical fluid (SCF) is a substance that is compressed beyond its critical pressure

and heated above its critical temperature (see Figure 2). Under this condition, the vapor and liquid phases become indistinguishable and the fluid behaves as a single phase having advantageous properties of both a liquid and a gas. Supercritical fluids have been widely used as foaming agents in the production of microcellular polymer foams (Tomasko *et al.*, 2003). Specifically, carbon dioxide and nitrogen have advantages of environmentally benign, being non-toxic and having relatively low critical temperature/pressure. Small amounts of supercritical fluids added to the polymer will result in dramatic changes in physicochemical properties, such as surface tension, viscosity, and solubility (Lee *et al.*, 1999).
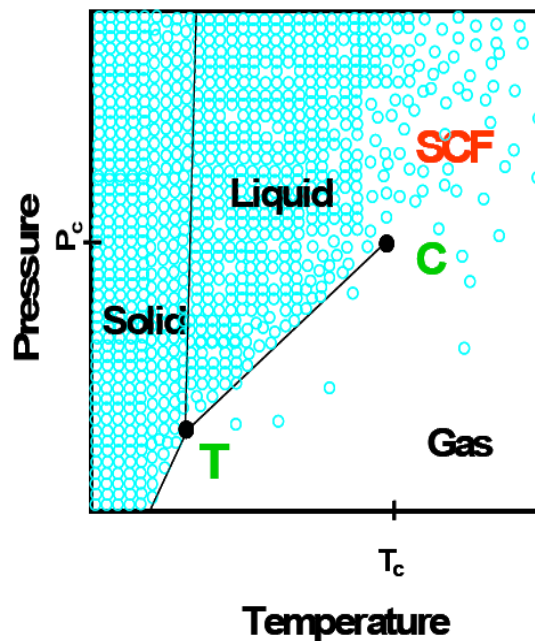
Fig. 2 Schematic pressure-temperature phase diagram for a pure component showing the supercritical fluid (SCF) region (H. Park, 2007)

There are many parameters such as the crystallinity of the polymer, the solubility of the

fluid in the polymer, the viscosity of the polymer melt, and the interfacial tension between

the polymers and the fluids, which determine the foaming quality. The crystallinity of the

polymer can be determined by Differential Scanning Calorimetry (DSC). More details will

be discussed in section 4.2 and 5.2. Solubility can be measured by Magnetic Suspension

Balance (MSB). (Yoshiyuki Sato *et al.*, 2000) Viscosity can be obtained by a rheometer

under different temperature and/or shear rate conditions.

This work focuses on the surface tension of polymers, which is one of the most important

parameters affecting the foaming and morphology of polymer products. This is because the

surface tension between the polymer melt and the fluid is a principal factor in determining

cell nucleation and growth (Myers D., 1991). In the foaming of polymer melts, the

homogeneous nucleation rate is described by $N_{\mathrm{hom}o}^{0} = C_0 f_0 \exp(-\Delta G_{\mathrm{hom}o} / k_B T)$ according

to bubble nucleation theories, where $N_{\mathrm{hom}o}^{0}$ is the number of nuclei generated per cm^3 per

second, C_0 the concentration of gas molecules (number of molecules per cm^3), f_0 the

frequency factor of the gas molecules, homo $\Delta G_{\mathrm{hom}o}$ the Gibbs free energy for

homogeneous nucleation, and k_B Boltzmann's constant (Cahn and Hilliard, 1959; Goel

and Beckman, 1994a). The Gibbs free energy ($\Delta G_{\mathrm{hom}o}$) for homogeneous nucleation is

given by $\Delta G_{\mathrm{hom}o} = 16\pi\gamma^3 / 3\Delta P^2$, where γ is the surface tension between the polymer phase

and nucleating bubble phase, and ΔP is the pressure difference across the polymer-gas

interface. When the surface tension of the polymer in the supercritical fluid decreases for a

little, the Gibbs free energy will be reduced by the cubic power of the change of surface

tension, and hence the nucleation rate will increase exponentially. Thus, generally low

surface tension is desired in the polymer foaming process, to increase the nucleation rate

and produce small and uniform cells (Nishioka *et al*., 1992).

2.2 Methods of Surface Tension Measurement

Measurement of interfacial or surface tension of polymer melts can be generally divided into two groups: static and dynamic measurements. Static methods (e.g., pendant drop, sessile drop, and spinning drop) are based on the equilibrium shape of the polymer drop in a force field (e.g., gravitational or centripetal). These methods require an accurate measurement of the density difference between the polymer and its gas environment. Long waiting time is needed before the equilibrium is reached due to the high viscosity of the polymers. This may as well cause the thermal degradation of the polymer. The dynamic methods follow the change in the shape of threads or elongated droplets to an equilibrium shape, including thread breakup, retraction of elongated droplets, and the dynamic shear rheometry on emulsions. The principles of static measurement techniques are briefly reviewed in the following sections. (H. Park, 2007)

Pendant drop method

Among all the methods of surface tension measurement, the pendant drop method is most commonly used for polymers and liquids. Although the theory of the pendant drop method is quite simply, experimental determination of the surface tension of a high viscosity polymer has been difficult, because of the handling of highly viscous polymer melts at high temperatures and pressures. (Demarquette *et al.,* 1994; Roe, *et al.,* 1967; Wu, 1970; Wu, 1982; Morita *et al.* 2002; Xue *et al.,* 2004)

Based on the pendant drop method, a molten polymer droplet is immersed into the bulk of another gas/fluid environment. The equilibrium drop profile is determined by the balance between drop gravity and polymer/fluids interfacial tension. The interfacial tension evaluated by the Laplace equation of capillarity can be determined from the input of the drop profile and the density difference across the fluid interface. This method has lots of advantages: no assumption about the rheological behavior of the component is made; it is useful for both Newtonian and viscoelastic fluids; it can be applied to liquid crystalline polymers; the interfacial tension is not disturbed during measurements; and the experiment setup is simple. On the other hand, the pendant drop method maintains the following potential problems: It requires the accuracy of the density differences of the materials and such information is rarely reported for polymeric materials. The density difference should be larger than 4-5% for polymer drops to reach the equilibrium shape in an acceptable time interval to avoid thermal degradation. (Lahooti *et al.* 1996)

The classical Laplace equation is the basis for all static measurements of interfacial and surface tensions. It states that the pressure difference across a curved interface can be described as:

$$\frac{\Delta P}{\gamma} = \frac{1}{R_1} + \frac{1}{R_2}$$

(1)

where R_1 and R_2 are the two principal radii of the drop, ΔP is the pressure difference across the curved interface, and γ is the interfacial tension.

The Axisymmetric Drop Shape Analysis (ADSA) approach is a pendant drop method; it relies on a numerical integration of the Laplace equation of capillarity to quantify surface tension. This numerical procedure applies to both sessile and pendant drops in shape

analysis (Cheng, P. *et al.*, 1990; Susnar, *et al.*, 1994; Cheng, P. *et al.*, 1992). Recently, ADSA has been used for determining polymer melt surface tension in supercritical fluids at high temperature and high pressure (Li, H. *et al.,* 2004). In this work, the related theory and experimental approaches of ADSA are introduced based on the surface tension measurement of polystyrene (PS) in supercritical CO_2 and high density polyethylene (HDPE) in supercritical N_2. The details of this technique are discussed as below.

In the absence of external forces, other than gravity, the pressure difference is a linear function of the elevation.

$$\Delta P = \Delta P_0 + \Delta \rho g z \tag{2}$$

In this expression, ΔP_0 is the pressure difference at a reference datum plane, $\Delta \rho$ is the difference in the density of the two bulk phases, g is the gravitational acceleration, and z is the vertical height measured from the reference plane.

When the axis x is tangent to the curved interface and normal to the axis of symmetry and the origin is placed at the apex as shown in Figure 3, the Laplace equation can be rewritten as:

$$\frac{d\phi}{ds} = \frac{2}{a} - \frac{\Delta \rho g}{\gamma} z - \frac{\sin\phi}{x} \tag{3}$$

Mathematically, the interface is described completely as u=u(x, y, z). Due to the symmetry in the system, this may be reduced to the description of the meridian section alone. A suitable representation of the meridian curve is in a parametric form:

$$x=x(s) \text{ and } z=z(s) \tag{4}$$

where s is the arc length measured from the origin. In this representation, both x and z are single-valued functions of s.

$$\cos\phi = \frac{dx}{ds} \tag{5}$$

A geometrical consideration yields the differential identities. And the boundary conditions:

$$x(0)=y(0)=z(0)=0 \tag{6}$$

from a set of first order differential equations for x, z, and φ as functions of the argument s. For given R_o and $\Delta\rho g/\gamma$, the theoretical drop given by the Laplace equation may be obtained by simultaneously integrating three equations.

Once an experimental drop profile is obtained, the ADSA-P program digitizes the image with sub-pixel resolution and randomly selects 20 coordinates. The profile is compared with the theoretical drop profile, using a least square algorithm with interfacial tension as one of the adjustable parameters. The best fit between these two profiles identifies the correct, i.e. operative, interfacial tension. The procedure is repeated 10 times for each experimental drop profile and 95% confidence limits are reported. For this work, typically 95% confidence limits are around ±0.01-$0.02mJ/m^2$.

Besides the drop profile coordinates, the input information required are the acceleration due to gravity and the density difference across the liquid-fluid interface. The details of numerical methods and procedures can be found elsewhere (del Rio, 1997).
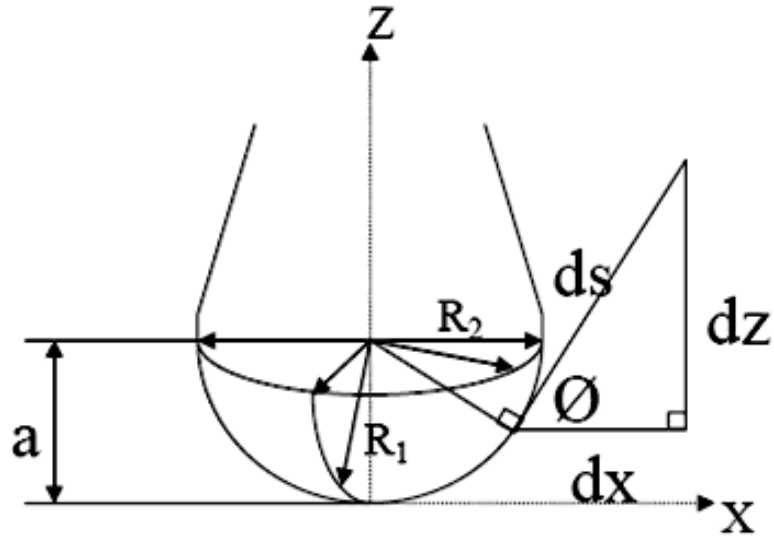
Fig. 3 Definition of the coordinate system of a pendant drop (H. Park, 2007)

Sessile drop method

The profile of the sessile drop is also that of a meniscus. The theoretical description of contact arises from the consideration of a thermodynamic equilibrium between the three phases: the liquid phase of the droplet (L), the solid phase of the substrate (S), and the gas/vapor phase of the ambient (V). The V phase could also be another liquid phase. At equilibrium, the chemical potential in the three phases should be equal. It is convenient to frame the discussion in terms of the interfacial energies. In Figure 4, we define the solid-vapor interfacial energy as γ_{sv}, the solid-liquid interfacial energy as γ_{sl} and the liquid-vapor energy (i.e. the surface tension) as γ_{lv}, we can write an equation that must be satisfied in equilibrium (known as the Young Equation): (F. Bashforth *et al.,* 1883)

$$\gamma_{sv} - \gamma_{sl} - \gamma\cos\theta_e = 0 \tag{7}$$
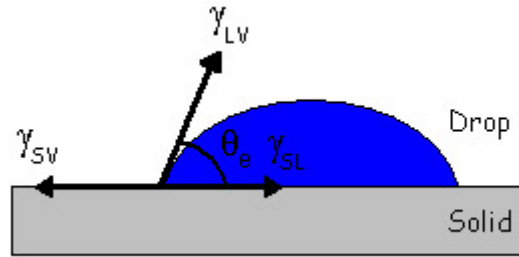
Fig. 4 An illustration of the sessile drop method with a liquid droplet partially wetting a solid substrate. θ_e is the contact angle, and γ_{sv}, γ_{lv}, γ_{sl} represent the solid-gas, gas-liquid, and liquid-solid interfaces, respectively.

To calculate the surface tension, the method is similar to that of the pendant drop method mentioned above. The form of the Laplace Equation is the same as the one for the pendant drop method in Eq. (3), except for a change in the sign of the gravitational term. (Adamson, A. W. *et al.,* 1997) An integration towards the three phase contact line (or point) provides a measure of the contact angle. (Lahooti, S, *et al.,* 1996; Cheng, P., *et al.,*1990; Cheng, P., *et al.,*1992; del Rio *et al.,* 1997) This method is more accurate than most other approaches, such as those based on goniometry.

Drop Weight Method

The procedure, in its simplest form, is to form drops of the liquid at the end of a tube, allowing the drops to fall into a container until enough have been collected to accurately determine the weight of a drop (J. Campbell, 1970). The method was devised by Tate in 1864, and a simple expression for the weight W of a drop is given by what is known as Tate's law (Adamson, A. W. *et al.,* 1997):

$$W = 2\pi r \gamma \tag{8}$$

where W is the weight of the drop and r is the inside radius of the tube. In employing this method, the tube should be ground smooth at the end and the drops should be formed slowly. γ, the surface tension can be obtained based on the equation.

Ring Method

This method is widely used and involves the determination of the force to detach a ring from the surface of a liquid. Like all detachment methods, one supposes that a first approximation to the detachment force is given by the surface tension multiplied by the periphery of the surface detached. Thus, the force balance, (J. Campbell, 1970)

$$W_{tot} = W_{ring} + 4\pi r\gamma \tag{9}$$

where W_{tot} is total weight, W_{ring} is the weight of the ring, r is the radius of ring, and γ is the surface tension. The surface tension is calculated from the diameter of the ring and the tear-off force.

Wilhemy Slide Method

This method is a popular and straightforward technique for measuring surface tension and static contact angles. It consists of putting a thin plate, such as a microscope cover glass or platinum foil microscope slide in the test fluid and measure the force acting on the plate when the system is at equilibrium. The basic observation is that the thin plate will support a meniscus. The force balance, (Adamson, A. W. *et al.,* 1997)

$$W_{tot} = W_{plate} + p\gamma \tag{10}$$

where W_{tot} is the total weight, W_{plate} is the weight of the plate, p is the perimeter and γ is the

surface tension. The surface tension is calculated from the diameter of the plate and the force acting on the plate.

2.3 Factors Affecting the Surface Tension

Surface tension of polymers in supercritical fluids varies with many parameters, e.g., system temperature, pressure, the molecular weight of the polymer, the solubility of the supercritical fluids, and the degree of crystallinity of the polymer.

Surface tension dependence on temperature and pressure above polymer melting point.
Temperature and pressure are two important parameters during the polymer foaming process. Recent work (H. Park et al., 2006; H. Park et al., 2007) showed several trends of the surface tension change with temperature and pressure for polymers above the melting points. In general, the surface tension decreases with increasing temperature and pressure. And there is a flattening of the surface tension versus temperature curves with increased pressure. Self-consistent field theory (SCFT) calculations were used to explain these experimental trends (H. Park *et al.,* 2007).

Correlation between solubility and surface tension. Besides surface tension, the solubility of a supercritical fluid in a polymer is also an important parameter in determining the foaming quality. By examining the change of solubility, as well as surface tension, with the change of temperature and pressure, one can see that both surface tension and solubility depend on temperature and pressure. In this work, the solubility of CO_2 in PS and N_2 in

HDPE at different temperatures and pressures will be compared and related with the change in the surface tension.

Surface tension of crystalline polymers during crystallization. The degree of crystallinity of a polymer can have a large impact on polymer properties. It is known that PS is a typical amorphous polymer, and HDPE is a typical crystalline polymer. Both types of polymers are often used in polymer microcellular foaming processes. In molten phase, crystalline polymers and amorphous polymers may behave similarly. When the temperature decreases below the melting point, amorphous polymers change into complete solid with disordered chain arrangements, but crystalline polymers would experience the process of crystallization: before a crystalline polymer turns into completely solid, it enters a viscoelastic state, where micro-crystals form and grow into regions of ordered chain arrangements within a continuous polymer melt. Surface tension measurement as measured of polymers undergoing such a transition can help understand the different behavior between amorphous and crystalline polymers (B. Wunderlich, 1958). It has been found that the surface tension of amorphous polymers at temperatures below the melting point does not change significantly. The surface tension of a crystalline polymer may behave differently from that of an amorphous polymer, i.e., the crystalline polymer may respond to variations of temperature below the melting point. How temperature change, or the rate of temperature change, affects the surface tension, as well as polymer crystallization, will be discussed in this work (B. Wunderlich, 1973; B. Wunderlich, 1980; H.G. Zachmann, 1964; T.F.J. Pijpers *et al.,* 2002).

Surface tension dependence on polymer molecular weight

The effect of molecular weight on polymer properties and processing has been well documented in the literature. Two monodisperse polystyrenes of different molecular weight and one polydisperse polystyrene were used to find the effect of polymer molecular weight on surface tension. Monodisperse polystyrene of a higher molecular weight has a higher surface tension under all experimental conditions. The surface tension dependence on temperature and on pressure is more significant for the higher molecular weight polystyrene than that of a lower molecular weight. For the polydisperse polystyrene, high surface tension values seem to be related predominantly to its high molecular weight portion of polystyrene molecules. (H. Park *et al.,* 2007)

It is generally the case that high molecular weight polymers will show a greater surface tension than low molecular weight polymers, all else being equal. The experimentally observed relationship is (R. A. L. Jones and R. W. Richards, 1999)

$$\gamma = \gamma(\infty) - c(1/M)^x \tag{11}$$

where γ is the surface tension, M is the molecular weight, $\gamma(\infty)$ is the surface tension for infinite molecular weight and c is a constant. The power x has been observed to be 2/3 for low molecular weight polymers, but switches to 1 for higher molecular weights. Self-consistent field calculations have been able to reproduce these low and high molecular weight regimes of polymer surface tension with molecular weight, and show that the transition between them is due to a depletion to effectively zero of the amount of polymer in the non-polymer side of the interface (R. B. Thompson *et al.,* 2008).

2.4 Surface Tension of Polystyrene in Supercritical Fluids

Previous work has shown the surface tension results of polystyrene with different molecular weight in supercritical CO_2 under different temperatures and pressures. Details are presented as follow. (H. Park, 2007)

2.4.1 Surface tension dependence on temperature and pressure above polymer melting point

This experiment was performed at five different pressures: 500, 1000, 1500, 2000, and 2500 psi, and five different temperatures: 170, 180, 190, 200, and 210°C. The surface tension value under various conditions was taken at its steady-state, when the change was less than $0.0001 mJm^{-2}s^{-1}$ for 1h. Thus the values obtained are regarded as equilibrium surface tensions. For each equilibrium surface tension reported, errors were on the order of 0.01 mJm^{-2}. Figure 5 shows the equilibrium surface tension values as a function of time. (H. Park, 2007)
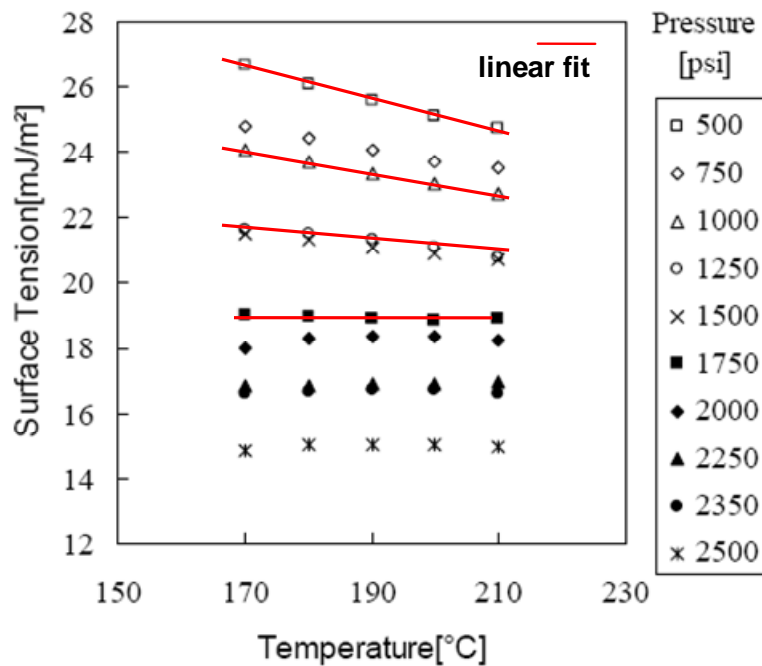
Fig. 5 The equilibrium surface tension of polystyrene in carbon dioxide at various temperatures (170, 180, 190, 200, 210°C) and pressures (500, 1000, 1500, 2000, 2500 psi). (H. Park, 2007)

It is apparent that at a given pressure, the surface tension decreases with increasing temperature; at a given temperature, the surface tension decreases with increasing pressure. The trend observed of the surface tension change with temperature is consistent with Wu's work (Wu, S., 1969). A second-order linear regression model was proposed and tested against the experimental results. (H. Park, 2007):

$$\gamma = 38.7032 - 0.0559\ T - 0.0100\ P + (2.596 \times 10^{-5})TP \tag{12}$$

$$(170°C < T < 210°C,\ 500\ \text{psi} < P < 2500\ \text{psi})$$

where the surface tension of polystyrene in supercritical CO_2 γ is in mJ/m^2, the temperature

T in ℃, and the pressure P in psi. Note that the second-order term in T or P is absent; statistically, γ is linearly related to T and P. However, there is an interaction term in TP, indicating γ dependence on T or P is affected by P or T, respectively. This indicates that, for polymer melt processes, one has to adjust both T and P to control the value of γ.

From Eq. (12), the following equations can be derived:

$$\frac{\partial \gamma_{PS}}{\partial P} = -1 \times 10^{-2}$$
(13)

$$\frac{\partial \gamma_{PS}}{\partial T} = -5.6 \times 10^{-2}$$
(14)

$$\frac{\partial^2 \gamma_{PS}}{\partial T \partial P} = 2.6 \times 10^{-5}$$
(15)

There are three main experimental trends presented in Eqs. (13) to (15). These are the dropping of the surface tension as a function of temperature for the pressure being less than ~2153 psi, the dropping of the surface tension with increasing pressure for the temperature being less than ~ 385°C, and the flattening of the surface tension versus temperature curves with increased pressure (see the fit lines in Figure 5). Self Consistent Field Theory (SCFT) was used to explain these experiment trends. (H. Park, 2007) We summarized it in Appendix A.

2.4.2 Surface tension measurement under glass transition temperature of PS

We already know that surface tension of a PS melt in CO_2 increases with decreasing temperature. But when the temperature is further decreased, sudden changes of surface tension are shown around 100°C in Figure 6, which is the glass transition temperature of the sample (Royer, J. R. *et al.,* 2000, Utracki, L. A., 2007). This is because once the temperature

goes below 100 ºC, PS solidifies and hence surface tension detected by ADSA would not change any further. The glass transition temperature of amorphous polymers could be measured by differential thermal analysis, e.g., differential scanning calorimetry (DSC). Now, this surface tension measurement can also be applied to measure the glass transition temperature of amorphous polymers. (H. Park, 2007)
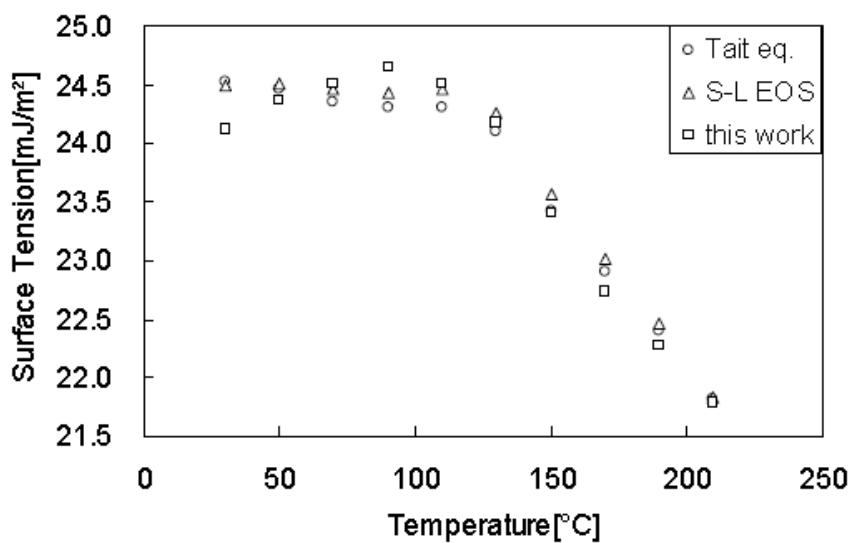
Fig. 6 Surface tension of PS through its glass transition temperature (H. Park, 2007)

2.4.3 Effect of molecular weight on the surface tension

The surface tension of polystyrene melts in supercritical nitrogen was measured at four different pressures, 500, 1000, 1500 and 2000 psi, and five different temperatures, 170, 180, 190, 200 and 210 °C. The equilibrium surface tension values for two monodisperse polystyrenes of M 100 000 and 400 000, along with a polydisperse polystyrene were obtained. The results showed that the higher molecular weight polystyrene has a higher

21

surface tension under all pressure and temperature conditions tested. The cross interaction between temperature and pressure effects is also more significant for the higher molecular weight polystyrene. (H. Park *et al.,* 2007)

2.4.4 Effect of Polydispersity on the Surface Tension

Similar to its monodisperse counterparts, the polydisperse polystyrene demonstrates three trends of surface tension variation: the polydisperse polystyrene has a higher surface tension than the monodisperse polystyrene of M 400 000, even though its molecular weight is below 400 000. In a polydisperse polymer, a wide distribution of molecular weights exists; thus, it may not be surprising that a portion of polystyrene molecules possesses a molecular weight greater than 400 000. This large molecular weight portion of polystyrene molecules may contribute more influentially to a high surface tension. In other words, high surface tension values are mainly derived from polystyrene molecules of high molecular weights. (H. Park *et al.,* 2007)

2.5 Polymer Crystallinity

Polymers exhibit two types of morphology in the solid state: amorphous and semicrystalline. In an amorphous polymer, the molecules are oriented randomly and are intertwined, as shown in Figure 7 (a), and the polymer has a glasslike, transparent appearance. Semicrystalline polymers contain both crystalline and amorphous regions in the same sample. The molecules packed together in ordered regions, as shown in Figure 7 (b), are called crystallites. In between these ordered regions, molecules are arranged in a random

disorganized state and these are called amorphous regions. Semicrystalline polymers tend to form very tough plastics because of the strong intermolecular forces associated with close chain packing in the crystallites. Also, because the crystallites scatter light, they are more opaque. Figure 8 shows the morphology of the amorphous polymer PS (a) and the crystalline polymer HDPE (b) as seen under a microscope. It can be found that unlike PS which is completely disordered, HDPE has some ordered lamellas in its solid state.

(a)   (b)

Fig. 7 Morphology of (a) amorphous and (b) semicrystalline polymer in the solid state

(a) PS   (b) HDPE
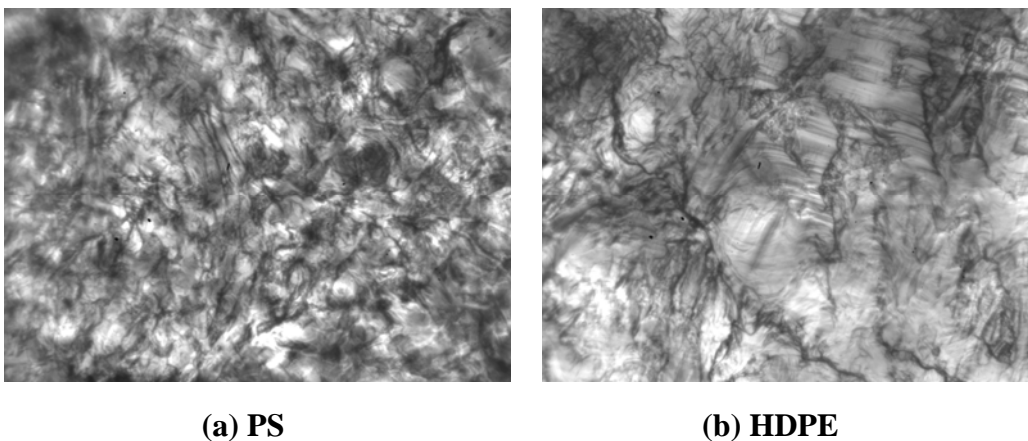
Fig. 8 Morphology of (a) PS and (b) HDPE in the solid state under a microscope

When the semicrystalline polymer melt solidifies, crystals begin to form and the point where it occurs is the nucleation point. The crystals increase in size by the progressive addition of atoms and grow until they impinge upon an adjacent growing crystal. In engineering materials, a crystal is usually referred to as a grain. A grain is merely a crystal without smooth faces because its growth was impeded via contact with another grain or a boundary surface. The interface formed between grains is called a grain boundary (the process is shown in Figure 9). (B.M. Epelbaum *et al.,* 2005)

(a)	(b)	(c)	(d)
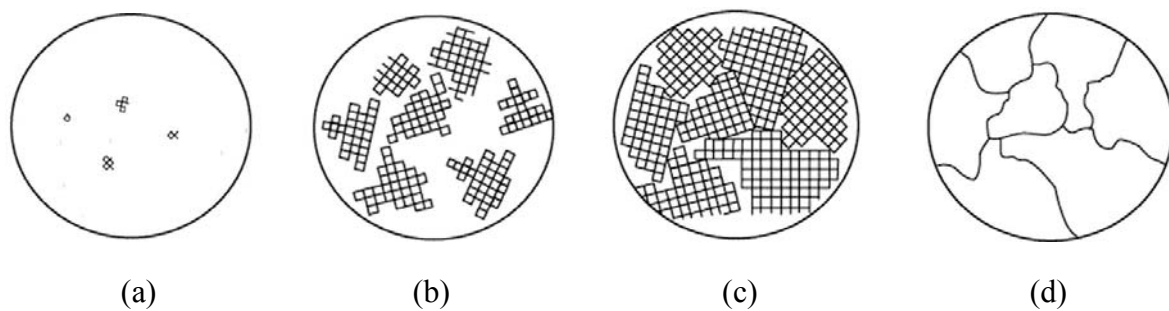
Fig. 9 Polymer Crystallization Process a) Nucleation of crystals, b) crystals growth, c) irregular grains form as crystals grow together, d) grain boundaries

Crystallinity is an indication of the amount of crystalline region in a polymer with respect to the amorphous content. As mentioned in the earlier section, polymer crystallinity is an important parameter in determining the surface tension and foaming quality, since crystallinity affects physical properties, such as storage modulus, permeability, density, and melting point. Differential scanning calorimetry (DSC) provides a rapid method for

determining polymer crystallinity through the measurement of the enthalpy of fusion and its normalization to the enthalpy of fusion of 100 % crystalline polymer. Precision is typically a few percent. (B. Wunderlich, 1990)

2.6 HDPE-Clay Nanocomposites

In the past decade, the use of nanometer-sized, layered silicate particles (i.e. the use of clay to reinforce polymers) have garnered a great deal of attention. Polymer nanocomposites have layered clay particles that are dispersed at a nanoscale level in the polymer matrix. Adding a small amount of clay can dramatically improve a wide variety of properties of the polymer matrix. The approach is to disperse individual, nanometer-sized, layered silicates in a molten polymer to create a clay-plastic nanocomposite. (Giannelis, E.P., 1996; Krishnamoorti, E. *et al.*, 1996; Kojima, Y. et al., 1993; Wang, K.H. *et al.*, 2002; Wang, K.H. *et al.*, 2001)

In recent works, high density polyethylene–clay nanocomposites (HNC) were prepared using an intermeshing and co-rotating twin-screw extruder. It was demonstrated that in comparison with pure HDPE, nanocomposites produce much finer and more uniform cell structures in the polymer foaming process. Additionally, an attempt to produce a nanocellular structure was successfully performed using HDPE–clay nanocomposites (Y. H. Lee *et al.,* 2005). Here, nanosized particles (clay) work as foreign nucleation sites, modifying the surface to enhance the interaction with the foaming agent, and they prevented cell coalescence during cell growth, which in turn led to an increase in cell density. Certain properties, such as fire retardance, barrier resistance, and thermal insulation can be

improved.

Until now, very few studies have reported the change in surface tension that occurs with the addition of clay to the pure polymer. This work will show the relationship between the surface tension and the concentration of the clay. The results will be compared with polymer crystallinity as well.

Chapter 3

Experimental Approaches

3.1 Materials

Pure HDPE and HNC are the polymers we used in this work. Figure 10 shows the morphology of (a) pure HDPE and (b) 0.5% HNC under microscope.

High Density Polyethylene. High Density Polyethylene (Nova Chemicals, Calgary, Canada, melt flow index (MFI) = 5.0 g/10 min (ASTM D 1238))

High Density Polyethylene –Clay Nanocomposite (HNC). The mixture of HDPE and 0.5 wt%, 3wt%, 5wt% organoclay, natural montmorillonite layered silicate modified with dimethyl dehydrogenated tallow alkyl ammonium (Cloisite 20A; Southern Clay Products, Gonzales, TX) was produced by Microcellular Plastics Manufacturing Laboratory at University of Toronto. (Y. H. Lee *et al.,* 2007)

Nitrogen. Nitrogen of 99.99% purity was purchased from Praxair (Danbury, CT, USA).
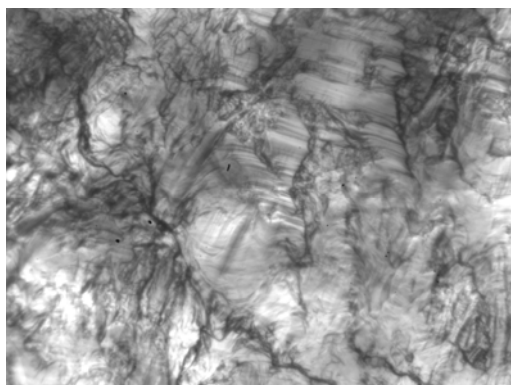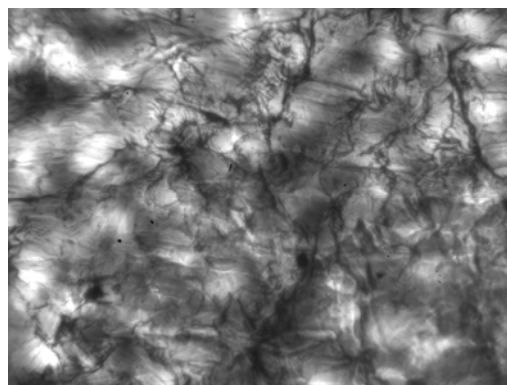
(a) HDPE　　　　　　　　　　　**(b) HNC0.5%**

Fig. 10 Morphology of pure HDPE (a) and 0.5% HNC (b) under microscope

3.2 Density Determination

The density of polymers not only is an input parameter for the determination of the surface tension of polymers in the Axisymmetric Drop Shape Analysis (ADSA) method, but is also important in the understanding of many polymer physics and engineering processes. However, density measurements are limited, time consuming and costly (Lau, W. *et al.,* 1973; Alexopoulos, A. H. *et al.,* 1989; Song, B. *et al.,* 1996). In previous research work, the sessile drop was employed to measure the surface tension and density simultaneously at high temperature (Anastasiadis, S. H. *et al.,* 1986).

The fact that the gas dissolution in the polymer melts caused volume swelling in the polymer melts must be considered for accurate solubility measurement and density calculation. The dilation of polymer samples caused by the plasticization effect of supercritical fluids was typically investigated at relatively low temperatures (Shenoy, S. L. *et al.,* 2003) because of the difficulty associated with the experiments at elevated temperatures and pressures. Therefore, it is a common practice to account for and predict the volume swelling at high temperatures of polymer melts using a thermodynamic approach, that is, the Equation of State (EOS). Among the equations of state, the Tait equation, the Sanchez and Lacombe (SL) EOS, the Simha and Somcynsky (SS) EOS are well known for predicting the density of polymers.

In a Tait equation method (Hess, M., 2004; Quach, A. *et al.,* 1971; Zoller, P. *et al.,* 1976), the parameters for polymers in supercritical fluids are:

$$v_p = v_0[1 - 0.0894\ln(1 + \frac{P}{B(T)})] \tag{12}$$

where v_p is the specific volume (cm^3/g), P is the pressure,

$$v_0 = 0.7884 \exp(5.79 \times 10^{-4} T)$$
$$B(T) = 887.2 \exp(-4.323 \times 10^{-3} T)$$
(13)

Sato et al. employed the Sanchez and Lacombe (SL) equation of state (EOS) to calculate the solubility of gases at high pressures and temperatures (Sanchez, I. C. and Lacombe, R. H., 1976; Sanchez, I. C. and Lacombe, R. H., 1978). The densities of polymers saturated with supercritical fluids were also determined by the SL-EOS as expressed below:

$$\tilde{\rho}^2 + \tilde{P} + \tilde{T}[ln(1-\tilde{\rho}) + (1-1/r)\tilde{\rho}] = 0$$
(14)

where $\tilde{\rho}$ is the reduced density, $\tilde{P}$ is the reduced pressure, $\tilde{T}$ is the reduced temperature and r is the number of sites occupied by a molecule; they are defined as

$$\tilde{P} = \frac{P}{P^*}, \tilde{\rho} = \frac{\rho}{\rho^*}, \tilde{T} = \frac{T}{T^*}, r = \frac{MP^*}{RT^*\rho^*}$$
(15)

where ρ is the density, P is the pressure, T is the temperature, M is the molecular weight and R is the gas constant. In the equation, the characteristic parameters, P^*, ρ^*, and T^*, of the SL-EOS for the mixture were evaluated using the following mixing rules:

$$P^* = \sum_i \sum_j \phi_i \phi_j P_{ij}^*, P_{ij}^* = (1 - k_{ij})(P_i^* P_j^*)^{0.5}, T^* = P^* \sum_i \frac{\phi_i^0 T_i^*}{P_i^*}$$
$$\frac{1}{r} = \sum_i \frac{\phi_i^0}{r_i^0}, \phi_i^0 = \frac{(\phi_i P_i^* / T_i^*)}{\sum_j (\phi_j P_j^* / T_j^*)}, \phi_i = \frac{w_i / \rho_i^*}{\sum_j w_i / \rho_i^*}$$
(16)

where T_i^*, P_i^*, ρ_i^*, and r_i^0 represent the characteristic parameters of the component i in its pure state.

Recently, the Simha and Somcynsky (SS) EOS was employed by Li et al. to predict the PVT behavior of polymer/gas mixtures, and the results were compared with those obtained from the SL-EOS (Li, G. *et al.,* 2006; Li, G. *et al.,* 2004). The SS-EOS is expressed as below (Simha, R. and Somcynsky, T., 1969):

$$\tilde{\rho}\tilde{V}/\tilde{T} = (1-\eta)^{-1} + \frac{2yQ^2(1.011Q^2 - 1.2045)}{\tilde{T}} \tag{17}$$

$$(\frac{s}{3c})[\frac{s-1}{s} + \frac{\ln(1-y)}{y}] = \frac{\eta - 1/3}{1-\eta} + \frac{y}{6\tilde{T}}Q^2(2.409 - 3.033Q^2) \tag{18}$$

Where $\tilde{\rho}$, $\tilde{V}$, $\tilde{T}$ are the reduced density, volume and temperature respectively; y is the occupied lattice site fraction; s is the number of segments dividing a molecule; c is the volume-dependent degrees of freedom; Q and η are defined as:

$$Q = (y\tilde{V})^{-1}, \eta = 2^{-1/6}yQ^{1/3} \tag{19}$$

During this procedure, the density difference between HDPE and nitrogen was determined by the Sanchez and Lacombe (S-L) equation of state (EOS). The data of density difference between HDPE and nitrogen at different temperatures and pressures are shown in Appendix B.

3.3 Experimental Setup

Axisymmetric Drop Shape Analysis-Profile (ADSA-P): Surface Tension Measurement.
ADSA-P was developed to determine liquid-fluid interfacial tensions. In this technique, images of the pendant drops were digitized with sub-pixel resolution and experimental drop profiles were compared with theoretical ones given by the Laplace equation. Other parameters, such as drop volume, surface area, and radius of curvature, can also be obtained. The ADSA-P method was employed for the surface tension measurement in this study. An example of the rough data obtained by this method is given in Appendix C.

The apparatus for this research was developed in a recent work. (H. Park, 2007) It consisted a high-temperature and high-pressure sample cell, in which a pendant drop was

formed. The cell was connected with an electrical band heater and a pressure pump to simulate the polymer foaming conditions and a data acquisition system with a PC was used to compute the interfacial tension from the drop profile. Figure 11 shows the schematic diagram of the ADSA-P experimental setup. The optical viewing cell (5), where the melt sample was formed, has two sapphire windows, mounted perpendicular to the cell axis. It is believed that the distortion of the sapphire window under pressure of less than 30Mpa is negligible. (H. Park, 2007)
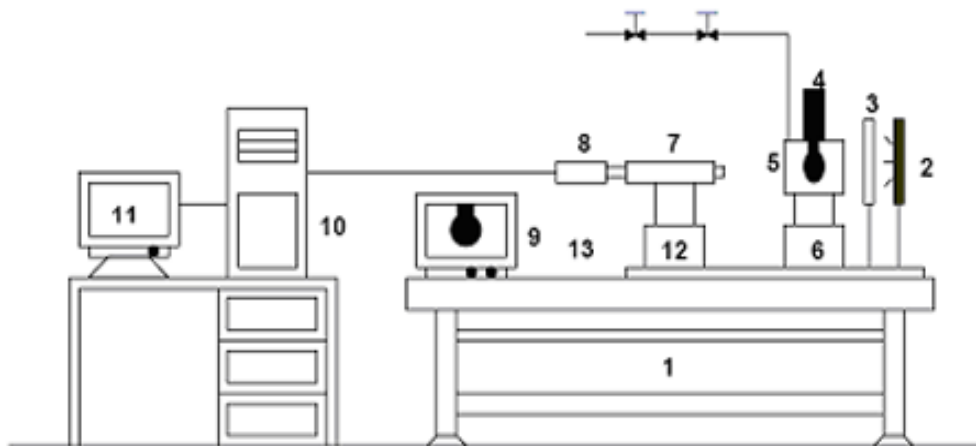
1.Vibration free table 2.Light source 3.Light diffuser 4.Feeding/holding rod for melts

5.View cell with heater 6.XYZ stage 7.Microscope 8.CCD Camera

9.Monitor 10.Computer 11.Monitor 12.XYZ Stage 13.Optial rail

Fig. 11 Schematic diagram of the ADSA-P experimental setup (H. Park, 2007)

Differential Scanning Calorimetry (DSC): Melting and Crystallization Measurement.

DSC was used to study the melting behavior and crystallization of HDPE as well as to determine the crystallinity of HNC. A DSC Q2000 V24.3 instrument was adopted, calibrated for temperature and enthalpy before use, with the melting point of high purity lead. Nitrogen at 20 ml/min was used as the purge gas. The melting/crystallization process of HDPE and HNC was monitored at different temperature increasing/decreasing rates. The crystallinity of HNC was calculated from the specific heat required for melting of the sample by integrating the corresponding peak and dividing this value (Hm) by the heat of fusion (293 J/g) for the pure crystalline phase of HDPE (Wunderlich, B. and Czornyj, G., 1977).

3.4 Stability of the Polymer Drops

Figure 12 shows a typical pendant drop image of the polymer melt in supercritical fluid taken by this system. (H. Park, 2007)
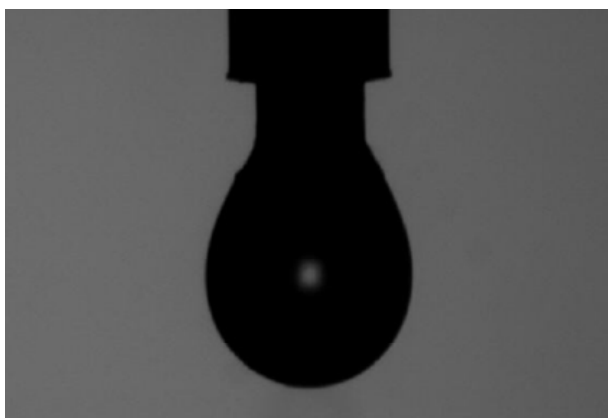
Fig. 12 A typical pendant drop image of the polymer melt in supercritical fluid

The polymer pellet size has to be determined before being attached to the rod. This is because the stability of the polymer drop is balanced by its gravity and surface tension. If the drop sizes are too large, the pendant drops are unstable and breakage may occur because of the dominant gravity. However, when the drop was smaller than a certain critical volume, the drop liquid may climb up along the feeding rod.

The stability of the polymer pendant drop is found to be related to the Bond number, (H. Park, 2007) by the expression

$$B_0 = \frac{\Delta \rho g R^2}{\gamma} \tag{20}$$

where $\Delta\rho$ is the density difference between two phases; g is the gravitational acceleration; R is the drop radius; and γ is the interfacial or surface tension between the immiscible phases. The Bond number is the ratio of buoyancy force to surface force. The number is used to indicate whether breakage occurs or a stable pendant drop is maintained. Based on the experimental experience, one can calculate the stable range of the bond number to determine the size of the drop in order to avoid breakage and liquid climb-up. Although within the stable range, it was found that the surface tension of the polymer melt was not influenced by the volume of the sample, the empirical pellet mass was kept at ~6.5mg for all measurements considering a good stability.

3.5 Polymer Oxidation

It is reported that above a certain temperature which depends on the composition of the polymer and usually exceeds 200°C, the mechanism and regularities of polymer oxidation change markedly. The main reaction of peroxide radicals becomes decomposition with

33

formation of low-molecular radicals, activation energy decreases and the rate of oxygen consumption becomes directly proportional to the oxygen pressure. (Yu.A. Shlyapnikov and I.A. Serenkova, 1983)

Due to the deficiency of the designed chamber, we can not vacuumize the system before we start measuring the surface tension. That is why oxidation may occur when the temperature reaches a certain degree. Based on our empirical experiments, it was found that for pure HDPE obvious oxidation took place when the temperature reached ~200°C. With the addition of clay, HDPE-clay nanocomposites experienced a more severe oxidation which occurred at a lower temperature, around 170°C. Once the oxidation started, it continued as time went by. The measured surface tension increased with increase in temperature, or further degree of oxidation, as shown in Figure 13.
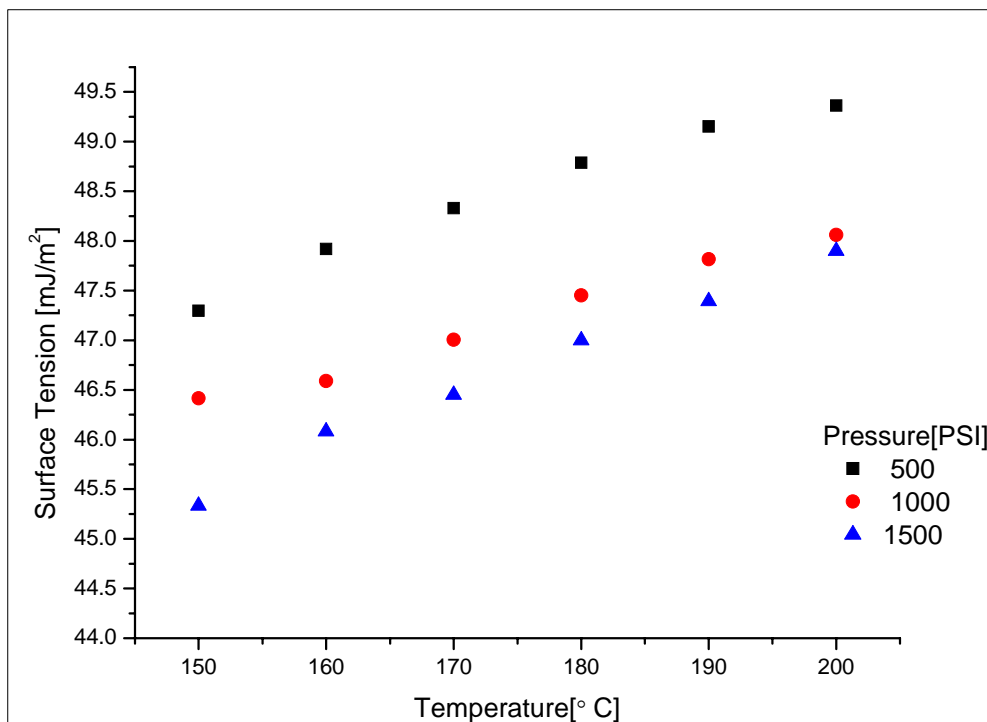
Fig. 13 Measured surface tension of a HDPE sample with oxidation

When taken out and viewed under the magnifying microscope as shown in Figure 14, it can be seen that compared to the pure sample, dark impurities showed up on the surface of the samples after the oxidation.

(a)   (b)
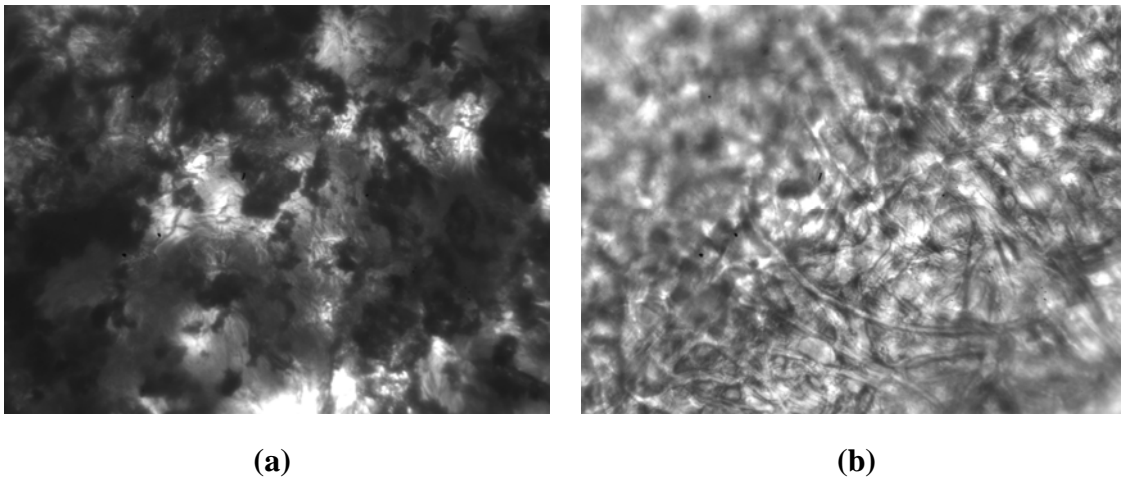
Fig. 14 The images of HDPE samples under microscope after the sample underwent the surface tension measurement in supercritical N_2 (a) with oxidation (b) without oxidation

To further look at the oxidation, one sample was kept in air under 210°C, and the surface tension was measured after 1 week. As shown in Figure 15, the measured surface tension is very scattered and extremely high up to ~125mJ/m^2, which is unreasonable and of course unreal. It is found that at this point the sample is completely dark and hard on the surface.

This is why the surface tension captured by ADSA is no longer available as the sample is not fluidic any more.
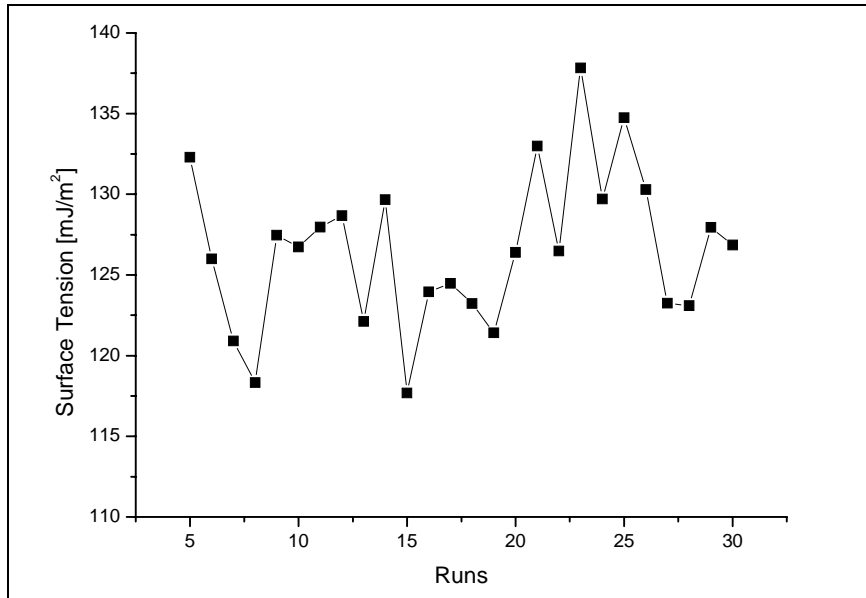
Fig. 15 Surface tension of a complete oxidized HDPE sample

To avoid the oxidation as much as possible, we have to maintain the sample in a nitrogen environment all the time. Based on our equipment, we charged the system with high pressure nitrogen for a few minutes before completely sealing the system, which in turn diluted the oxygen remaining in the chamber and thus minimized the oxidation.

3.6 Reproducibility

The reproducibility of the surface tension experiment was tested by measuring the surface tension of the polymer melts in N_2 at different temperatures and pressures. For a certain temperature and pressure, at least two runs were conducted. Figure 16 illustrates the surface

tension of the HDPE melts in N_2 at 170°C, 1000psi. The surface tension measurements
exhibited good consistency from run to run. For the crystallinity test, the polymer was
heated and cooled for two rounds, and the heat change during the second round melting was
used for the crystallinity calculation. Details will be explained in later sections. For each
concentration, several samples were tested to get an average value.
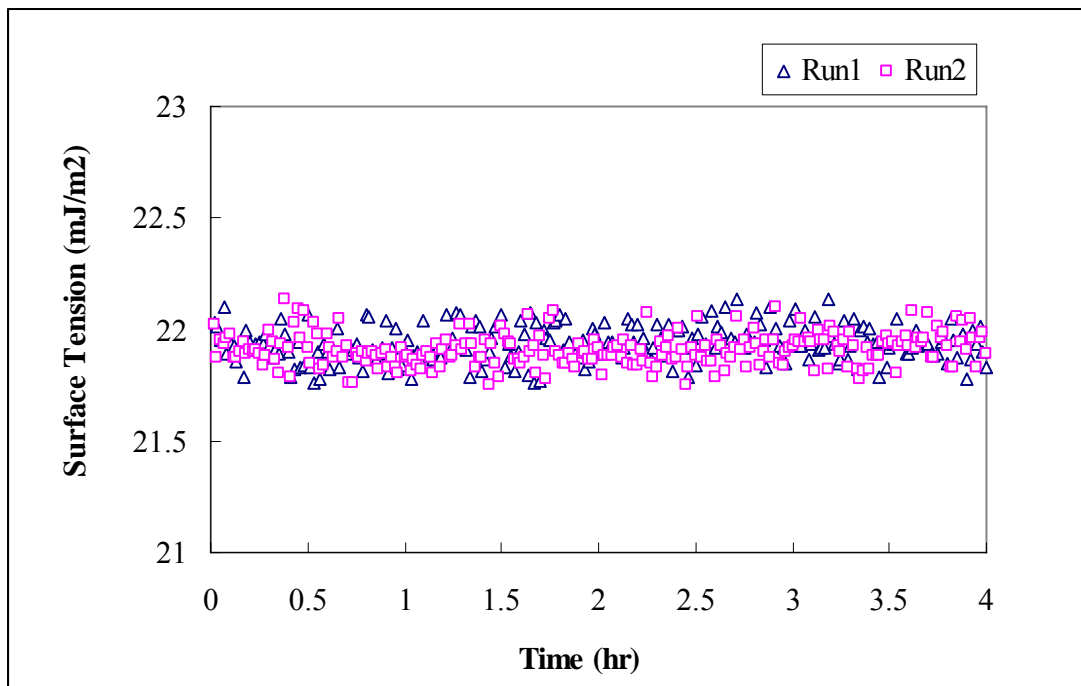
Fig. 16 Reproducibility test: results of two runs for the surface tension of HDPE in

N_2 at 170ºC, 1000psi.

Chapter 4*

Surface Tension of High Density Polyethylene in Supercritical Nitrogen

4.1 Objectives

The degree of crystallinity of a polymer can have a large impact on polymer properties. It is known that polystyrene (PS) is a typical amorphous polymer, and high density polyethylene (HDPE) is a typical crystalline polymer. Both types of polymers are often used in polymer microcellular foaming processes. In molten phase, crystalline polymers and amorphous polymers may behave similarly. This is not the case in the solid state. When the temperature decreases below the melting point, amorphous polymers change into complete solids with disordered chain arrangements, but crystalline polymers would experience the process of crystallization: before a crystalline polymer becomes completely solid, it enters a viscoelastic state, where micro-crystals form and grow into regions of ordered chain arrangements within a continuous polymer melt. Surface tension measurement of polymers undergoing such transitions can help clarify the different behavior between amorphous and crystalline polymers (Wunderlich, 1958). It has been found that the surface tension of amorphous polymers at temperatures below the melting point does not change significantly. But to date, no measurement on the surface tension of crystalline polymers has been made at temperatures below the melting point. It is plausible that the surface tension of a crystalline polymer may behave differently from that of an amorphous polymer, i.e., the crystalline polymer may respond to variations of temperature below the melting point. A follow up question would then be how temperature, or the rate of temperature change, affects the

---

*This chapter is based on the manuscript of the published paper on Colloids and Surfaces A

surface tension, as well as polymer crystallization.

The primary purpose of this work is to establish an ADSA-based approach for evaluating the surface tension of the crystalline polymer high density polyethylene (HDPE) in supercritical nitrogen over a wide range of temperatures and pressures. The relationships of surface tension, solubility and crystallization with temperature and pressure will be investigated. The results will be compared with those of the amorphous polymer polystyrene (PS), to show the difference between crystalline and amorphous polymers.

4.2 Experimental

4.2.1 Differential Scanning Calorimetry (DSC) Measurement: Melting and Crystallization of HDPE

DSC was used to study the melting behavior and crystallization of HDPE. The melting/crystallization process of HDPE was monitored at different temperature increasing/decreasing rates. For the melting process, the heating rates of 5 C°/min and 30 C°/min were used. For the crystallization process, the cooling rates were 3 C°/min, 30 C°/min, and 35 C°/min.

4.2.2 Surface Tension Measurement

The surface tension of HDPE in supercritical nitrogen was measured at different temperatures from 100 to 190 °C, within a wide range of pressures, from 500 to 1500 psi. The experimental setup was tested for its accuracy and reproducibility with a range of polymer-gas combinations, and the details of this setup and validation for the surface

tension measurement were described in a recent publication. (H. Park, 2006)

The technique of Axisymmetric Drop Shape Analysis-Profile (ADSA-P) was used for image analysis and parameter estimation. During this procedure, the density difference between HDPE and nitrogen was an input parameter, which was determined by the Sanchez and Lacombe (S-L) equation of state (EOS). The details of this technique and the calculations were described in Chapter 3, the experimental section.

Surface Tension of HDPE in N_2 above the Melting Point. This experiment was performed at eight different temperatures 125, 130, 140, 150, 160, 170, 180 and 190 °C above the HDPE melting point, ~125°C, and three different pressures 500, 1000, and 1500 psi. The surface tension value of HDPE in supercritical nitrogen under various conditions was taken at its steady-state, when the change in surface tension was less than $0.0001 mJm^{-2}s^{-1}$ for 1h. Thus the values obtained are regarded as equilibrium surface tensions. For each equilibrium surface tension reported, errors were on the order of 0.01 mJm^{-2}.

Steady-state Surface Tension of HDPE in N_2 during Crystallization. The system pressure was controlled at 500, 1000, or 1500 psi each time. The literature melting point for HDPE is around 125 °C, above which the polymer is liquid, and below which polymer starts to crystallize until it turns completely solid. To investigate the effect of HDPE crystallization, the system was cooled from 150 to 100 °C in intervals of 10 C°, during which the system was maintained at each condition for two hours, and the surface tension

value was measured at its steady-state in each interval.

Dynamic Surface Tension of HDPE in N₂ during Crystallization. HDPE was first melted at above 130 ℃ and kept at that temperature for 8 hours until the surface tension reached equilibrium. Then the temperature was steadily dropped from 130 ℃ to 110 ℃. It took about 15 minutes for the band heater to complete this procedure. The system temperature was maintained at 110 ℃ afterwards for 1 hour. The time-dependent, or dynamic, surface tension during this entire process was measured until the system reached the final stead-state, where the surface tension reached equilibrium at 110 ℃.

Correlation of Surface Tension Change with Temperature Change Rate. Two experiments were performed with different cooling procedures when crystallization of HDPE occurred. For the slower cooling rate experiment, the temperature was decreased from 150°C to 100°C stepwise in 10 C° intervals. The system was maintained at each interval until it reached steady-state and surface tension was measured. For the faster cooling rate experiment, the temperature was decreased from 150 °C to 100 °C steadily. The system was then maintained at 100 °C until it reached steady-state.

4.3 Results and Discussion

4.3.1 Melting Point of HDPE

The reported melting point of HDPE, ~ 125 °C, is in the range of 120 to 130 °C. To determine the melting point of the sample used in our experiments, differential scanning

calorimetry (DSC) was used. Figure 17 shows the DSC results of HDPE melting under different heating rates. The polymer starts melting at around 110 ºC. The peak point at the slower heating rate is found to be around 125 °C, which is considered the melting point of the sample.
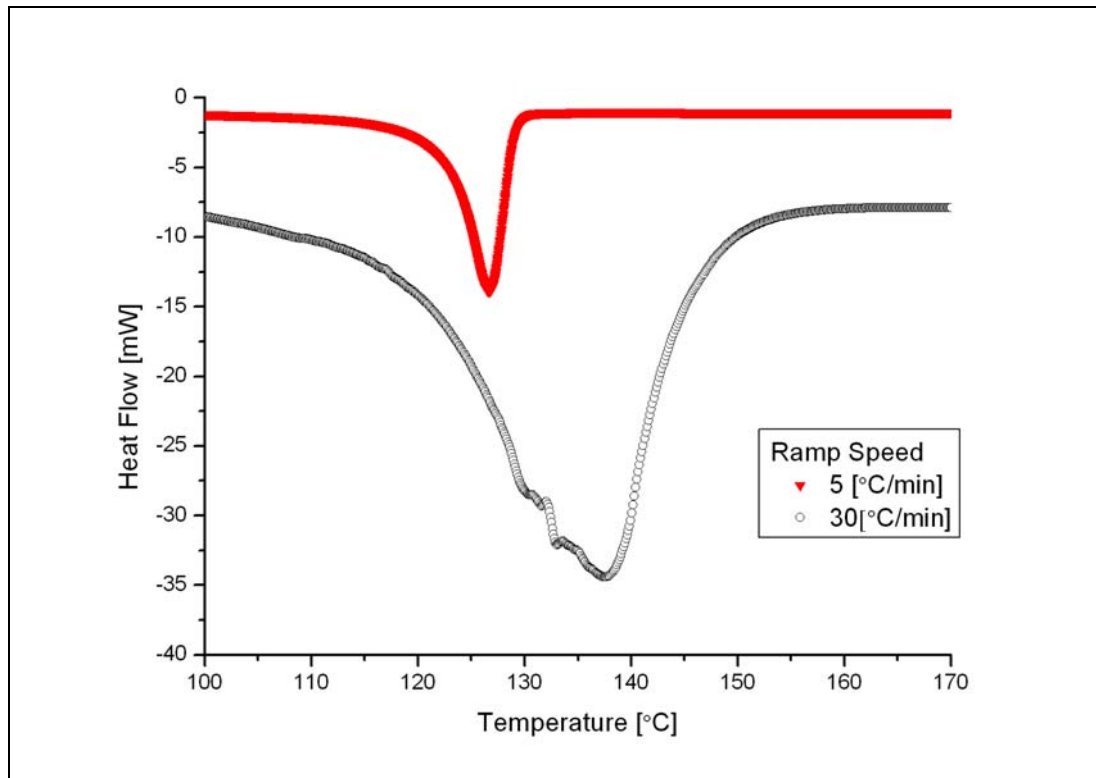
Fig. 17 DSC results of the melting process of HDPE at different heating rates: 5 ºC/min (solid symbols), 30 ºC/min (open symbols).

4.3.2 Surface Tension Dependence on Temperature and Pressure above Polymer Melting Point

The equilibrium surface tension value of the HDPE melt in supercritical nitrogen was measured under various temperatures and pressures. Figure 18 shows the equilibrium surface tension at each temperature and pressure.
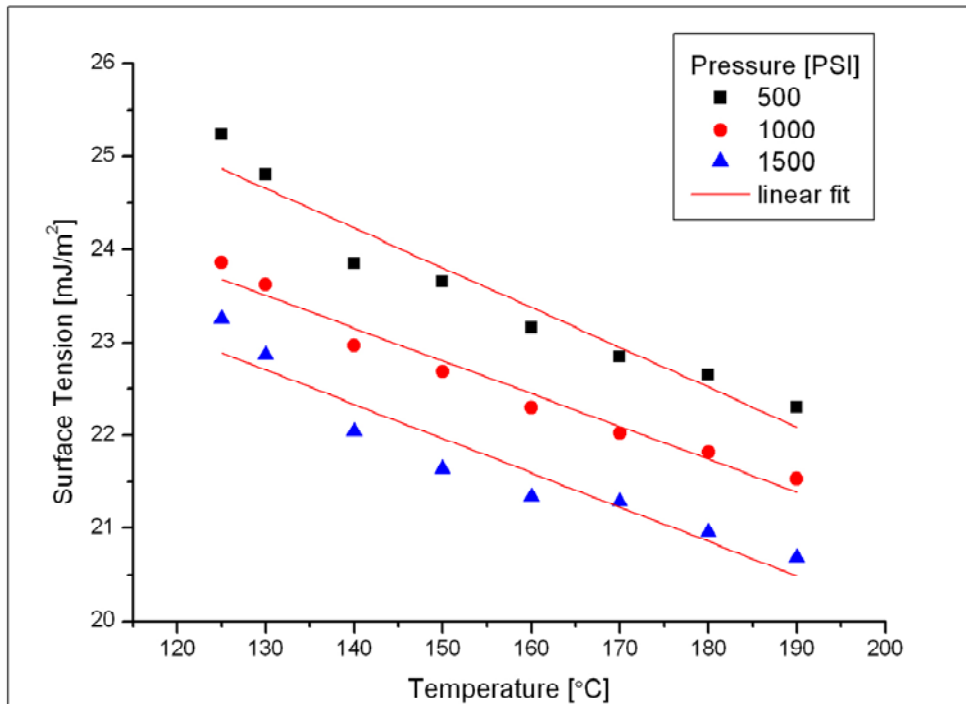
Fig. 18 The equilibrium surface tension of HDPE in N_2 at various temperatures (125, 130, 140, 150, 160, 170, 180, 190 ºC) and pressures (500, 1000, 1500 psi) above HDPE melting point (125 ºC).

The surface tension varies from 20.5 mJ/m^2 at 190 °C, 1500 psi, to 25.5 mJ/m^2 at 125 °C, 500 psi. It is apparent that at a given pressure, the surface tension decreases with increasing temperature; at a given temperature, the surface tension decreases with increasing pressure. The trend observed of the surface tension change with temperature is consistent with that of Wu, where a linear relationship between surface tension and temperature was proposed for polyethylene melts. (Wu, S., 1969) However, in our experiments, pressure was an additional

variable. To find how surface tension is related with both temperature and pressure, a linear regression model for the surface tension γ was proposed and tested against the experimental results.

$$\gamma = 31.7534 - 0.04611T - 0.00165P \tag{21}$$

$$(125 \text{ °C} < T < 190 \text{ °C}, 500 \text{ psi} < P < 1500 \text{ psi})$$

where the surface tension of HDPE in supercritical N_2 is in mJ/m^2, the temperature T in ºC, and the pressure P in psi. Table 1 shows analysis of variance, or ANOVA, indicating the validity of the regression model: the observed F-value is larger than the tabulated F-value at the 95% confidence level.

Table 1 ANOVA (Analysis of Variance) Table for a Linear Regression Model of HDPE in

N_2

	sum of square(SS)	degree of freedom	mean square(MS)
regression	27.35163	3	13.67581
residual	0.45054	17	0.02503
total	27.80217	20	
	F_{obs}=546.4; $F_{3,17,0.05}$=3.2, R-Square=0.98		

In Table 2, the validity of each parameter in the equation was also examined by using the t-test: all observed t values are greater than the tabulated t-value at the 95% confidence level. This result shows the second-order term in T or P and the interaction term in TP are absent; statistically, γ is linearly related to T and P.

Table 2 t-Test for Evaluating Each Parameter of the Proposed Linear Regression Model of HDPE in N_2

parameters	coefficients	standard error	|t-value|
intercept	31.75343	0.29090	109.15406
T	-0.04611	0.00173	26.71155
P	-0.00165	8.46E-5	19.47416
	$T_{0.025,17}$=2.11		

From Eq. (21), the following equations can be derived:

$$\frac{\partial \gamma_{HDPE}}{\partial P} = -1.65 \times 10^{-3} \qquad (22)$$

$$\frac{\partial \gamma_{HDPE}}{\partial T} = -4.61 \times 10^{-2} \qquad (23)$$

The trends of γ with T and P seem to be consistent with that of the surface tension of polystyrene (PS) in supercritical CO_2 (H. Park, 2007) reviewed in Chapter 2, where

$$\frac{\partial \gamma_{PS}}{\partial P} = -1.00 \times 10^{-2} \qquad (13)$$

$$\frac{\partial \gamma_{PS}}{\partial T} = -5.59 \times 10^{-2} \qquad (14)$$

$$\frac{\partial^2 \gamma_{PS}}{\partial TP} = 2.60 \times 10^{-5} \qquad (15)$$

There is one different trend for HDPE in N_2 from PS in CO_2, Eq. (15): the interaction term in TP for PS in CO_2 shows the rate of the surface tension change of PS with temperature increases with increasing pressure, while this term is absent for HDPE in N_2 indicating the rate of the surface tension change of HDPE with temperature does not change much.

4.3.3 The Change of Solubility with Temperature and Pressure

Besides surface tension, the solubility of a gas in a polymer is also an important parameter in determining the foaming quality. By examining the change of solubility, as well as surface tension, with the change of temperature and pressure, one can see that both surface tension and solubility depend on temperature and pressure.

First, if the temperature is maintained, as the pressure is increased, the solubility of N_2 in

HDPE increases and the surface tension decreases. This is reasonable when considering the

fact that an increase in gas-phase pressure will likely induce more gas dissolution into the

liquid phase (H. Park, 2006). Comparing the surface tension dependence on pressure, from

Eqs. (22) and (13), it is found the surface tension drops more with the same amount of

increase in pressure for PS in CO_2 than for HDPE in N_2. Correspondingly, the solubility

dependence on pressure of CO_2 in PS is stronger than that of N_2 in HDPE, which can be

observed from Eqs. (24) and (25) derived from the solubility data: (Yoshiyuki S., *et al.,*

1999; Lee, Y.H. *et al.,* 2005)

$$\frac{\partial C_{N_2}}{\partial P} = 7.5 \times 10^{-6} \tag{24}$$

$$\frac{\partial C_{CO_2}}{\partial P} = 2.86 \times 10^{-5} \tag{25}$$

From the experimental results, the surface tension at different temperatures begins to

converge at higher pressures for PS in CO_2, while this phenomenon is not observed for

HDPE in N_2. Figure 19 shows that the solubility of N_2 in HDPE increases slightly with

increasing temperature, while to the contrary, the solubility for CO_2 in PS decreases with

increasing temperature. For CO_2 in PS, there are two competing factors affecting the

solubility: an increase in pressure tends to increase the solubility, while an increase in

temperature tends to decrease it. Thus, pressure and temperature together determine the

solubility of CO_2 in PS. Based on the same argument, the rate of the surface tension change

of PS with temperature decreases at higher pressures (H. Park, 2006). For the case of N_2 in

HDPE, increases in both pressure and temperature tend to increase the solubility.

Correspondingly, the rate of the surface tension change of HDPE with temperature does not

decrease at higher pressures; note there is no interaction term for HDPE.
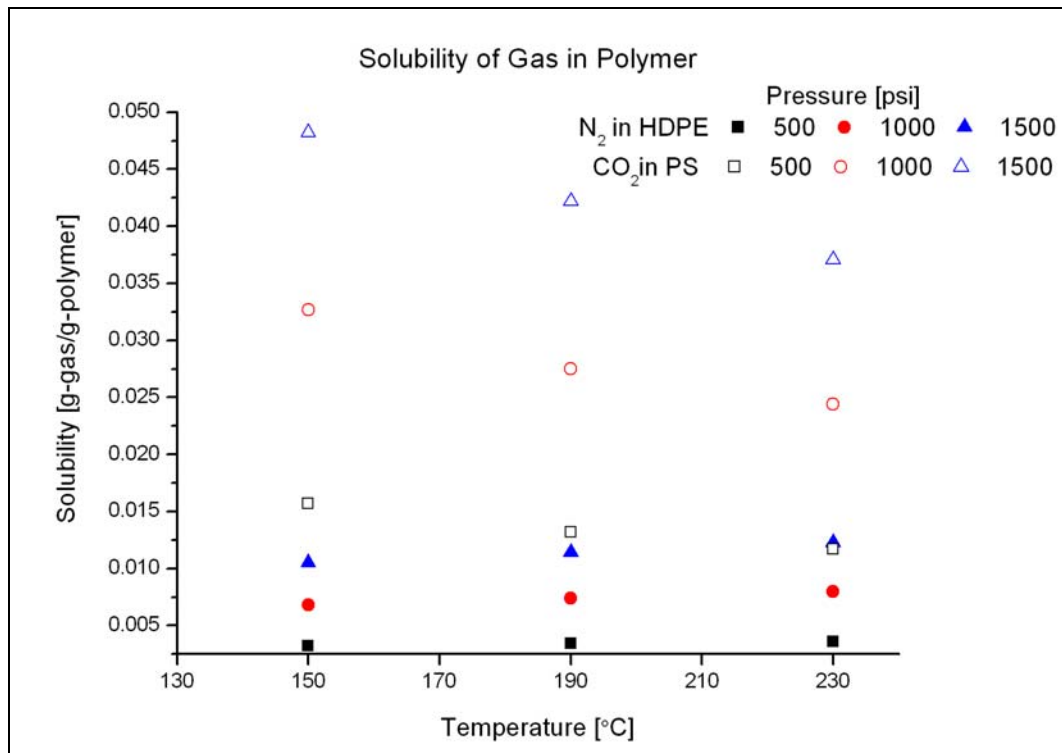
Fig. 19 Solubility of gas in polymer at various temperatures (150, 190, 230 ºC) and

pressures (500, 1000, 1500 psi): the solid symbols present the solubility data of N_2 in

HDPE, and open symbols present the solubility data of CO_2 in PS.

4.3.4 Surface Tension of HDPE in N_2 Accompanied by Crystallization

It has been found that the surface tension of amorphous polymers at temperatures below the melting point does not change significantly. It is plausible that the surface tension of a crystalline polymer may behave differently from that of an amorphous polymer, i.e., the crystalline polymer may respond to variations of temperature below the melting point. Thus, the surface tension of HDPE in N_2 during crystallization was measured. The results of experiments are shown in Figure 20.
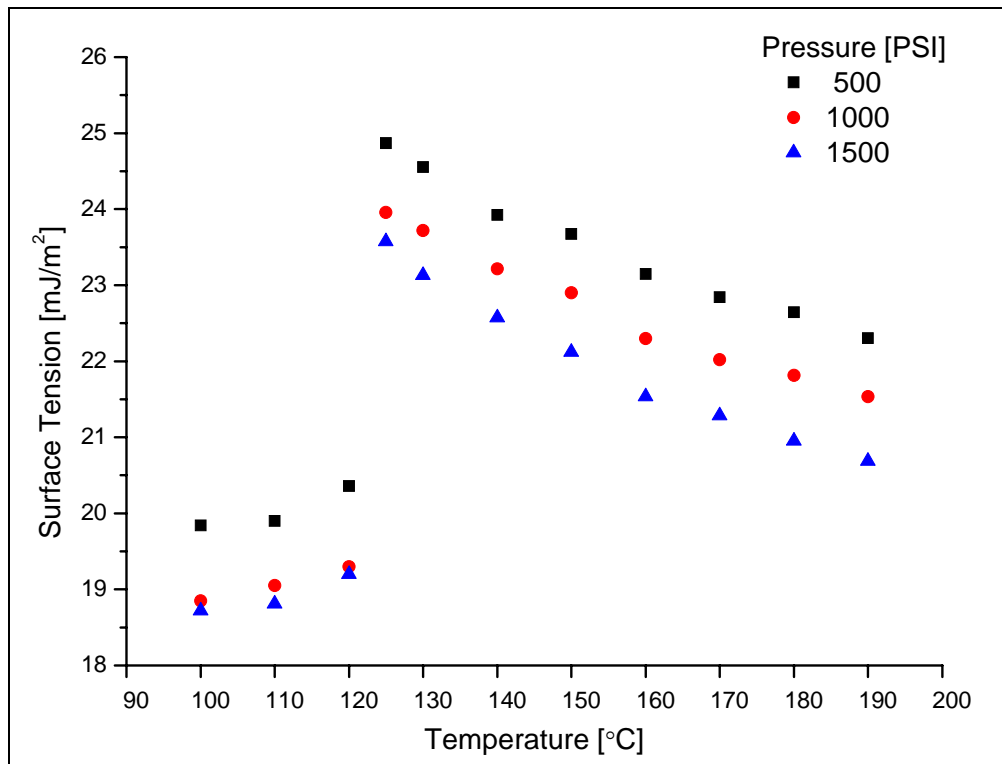
Fig. 20 The equilibrium surface tension of HDPE in nitrogen at various temperatures and pressures (500, 1000, 1500 psi) through its crystallization region. The system was cooled from 150 to 100 °C in intervals of 10 C°, during which the system was maintained at each condition for two hours, and the surface tension value was measured at its steady-state.

With decreasing temperature, the surface tension first increases until temperature reaches the melting point of HDPE, ~125 ºC, and then it drops sharply with further decreasing temperature. The surface tension eventually approaches a plateau, around 20 mJ/m^2 at 110 ºC for a pressure of 500 psi. The Differential Scanning Calorimetry results of melting HDPE show that the polymer starts to melt at 110 ºC. This may explain why the surface tension of HDPE does not change any further when temperature goes under 110 ºC, since the polymer becomes completely solid at this point and below. Note, surface tension of a PS melt in CO_2 increases with decreasing temperature, and it does not change any further when temperature reaches 100 ºC, which is the glass transition temperature of PS. If comparing the surface tension results of these two polymers under their melting points, one may consider that the difference is due to the fact that polystyrene is an amorphous polymer, while HDPE is a crystalline polymer. Once the temperature goes below 100 ºC, PS solidifies and hence surface tension detected by ADSA would not change any further. This is similar to the case of HDPE under 110 ºC. However, different from PS, there is a decrease in surface tension between 110 ºC and 125 ºC observed for HDPE, which is the period for crystallization. During the HDPE crystallization, there are micro-crystals nucleated that immerse in the polymer melt.

Polymer crystallization can take time and occur with a range of temperatures, during which the polymer behaves viscoelastically with a high elasticity characteristic. When temperature is decreased to induce crystallization, small crystals form and grow. These crystals may act as, or be considered, nanoparticles, in the polymer melt. It is known that the presence of nanoparticles in polymer melts enhances the polymer interaction with foaming

agents, which leads to an improved foaming quality. (Lee, Y. H. *et al.*, 2005; Lee, Y. H. *et al.*, 2007) In Chapter 5, results show that the surface tension is reduced when nanoparticals are added into the pure polymer. Thus, it may not be surprising that the surface tension decreases with decreasing temperature, when accompanied by the polymer crystallization.

A follow up question would be how temperature or the rate of temperature change, affects the surface tension, as well as polymer crystallization.

4.3.5 Correlation of Surface Tension Decrease with Temperature Change Rate

The dynamic surface tension was measured when temperature was steadily dropped from 130 ºC to 110 ºC, passing through its melting point 125 ºC. The results are shown in Figure 21.
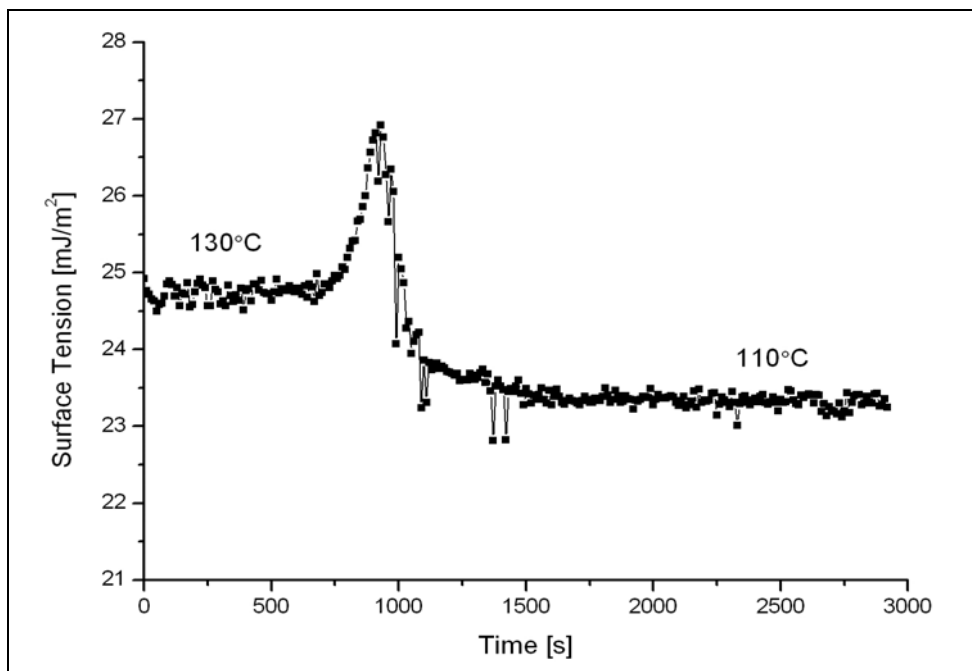
Fig. 21 Surface tension of the HDPE melt in supercritical nitrogen at different temperatures as a function of time when the temperature changes from 130 ºC steadily to 110 ºC. It took ~ 15 minutes for the band heater to complete this procedure. The temperature was then maintained at 110 ºC for 1 hour.

The surface tension first increases with decreasing temperature and then drops sharply, approaching a plateau around 23.3 mJ/m^2. During this dynamic process, the increase in surface tension with decreasing temperature at the beginning is due to the fact that the temperature is still above the HDPE melting point. Once the temperature goes below this melting point, HDPE starts to crystallize and thus there is a decrease in surface tension until it reaches a plateau. To recall the experiments discussed in the last section, where the temperature was dropped stepwise, the surface tension decreased to 20.0 mJ/m^2. But in the current continuous decrease in temperature, the surface tension only decreased to 23.3 mJ/m^2. An obvious difference in temperature change is the rate of decrease in temperature. It is concluded that the faster the temperature change rate, the smaller change in surface tension.

Figure 22 is the DSC results of HDPE crystallization under different temperature change rates.
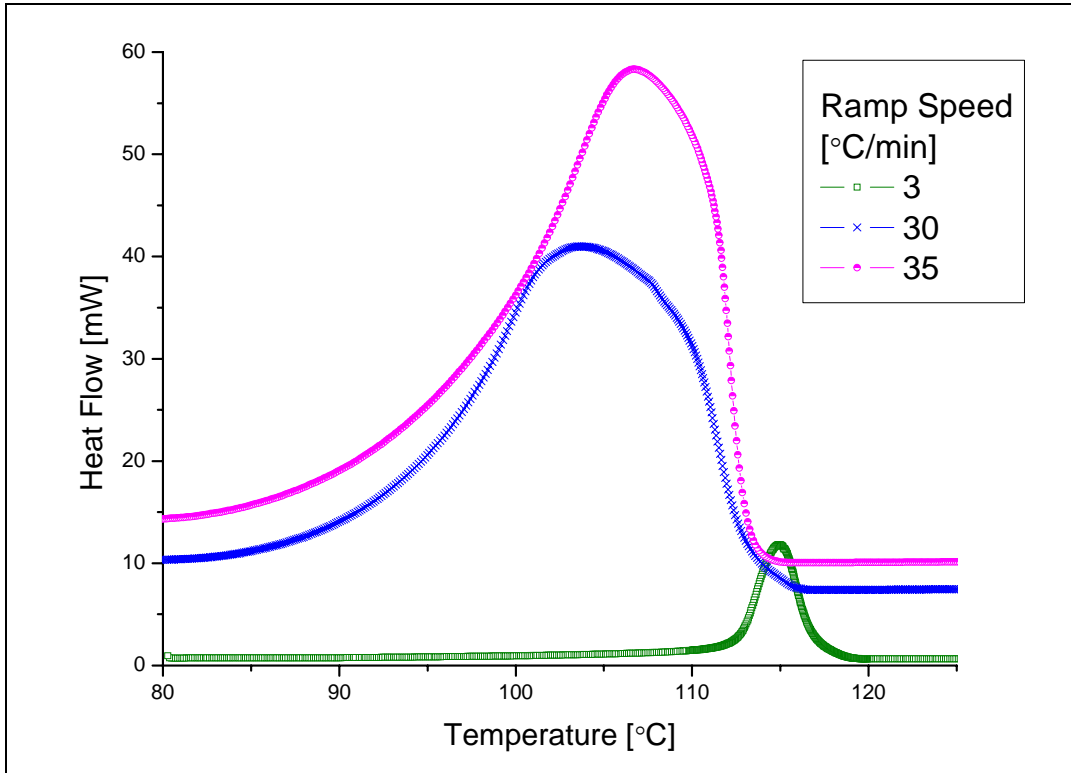
Fig. 22 DSC results for the crystallization process of HDPE at different cooling rates: 3 ºC/min, 30 ºC/min, 35 ºC/min.

It shows that if the polymer is cooled down slowly, HDPE has enough time to crystallize, and thus more crystals can form and grow. This in turn results in a greater decrease in surface tension. To the contrary, if the temperature change rate is high, HDPE does not have enough time to crystallize before becoming completely solid, corresponding to a broader peak at a lower temperature. Thus, less of a decrease in surface tension is observed.

Two experiments were conducted at different temperature change rates to confirm this argument. The results are shown in Figure 23.
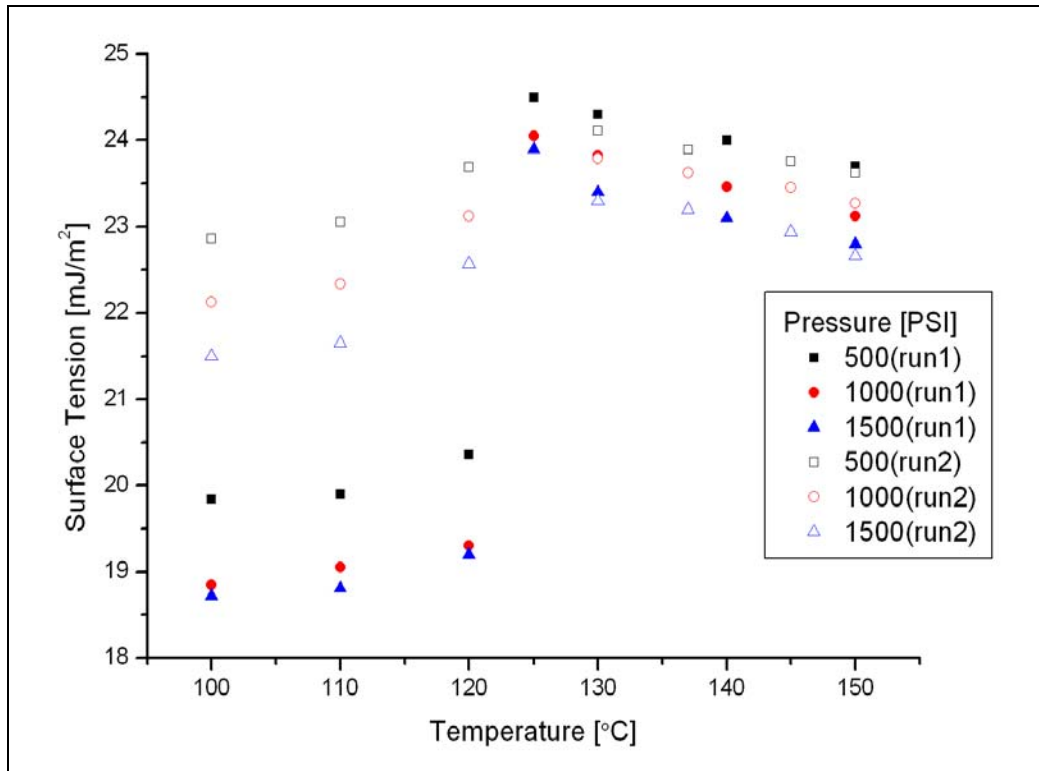
Fig. 23 The surface tension of HDPE in Nitrogen at different temperature change rates: the solid symbols indicate experiments at slower crystallization cooling speeds. The open symbols indicate experiments at faster crystallization cooling speeds.

The surface tension of HDPE in nitrogen at different temperature change rates was measured. The solid spots were the surface tension values obtained at the slower temperature change rate, while the open spots were obtained at the faster temperature change rate. It is seen that the faster a temperature change rate, the less a decrease in surface tension. Figure 24 shows the appearance of the polymer after the process of crystallization at different temperature change rates.

(a)   (b)
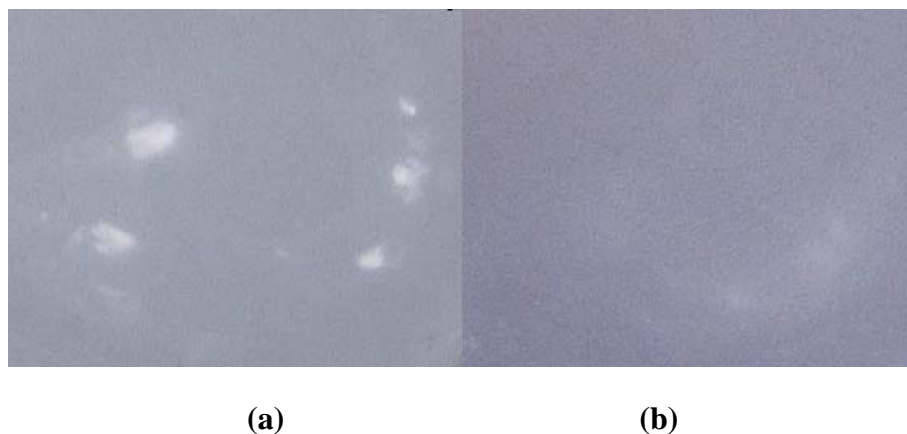
Fig. 24 The images of HDPE samples under 40 times microscope after the sample underwent different crystallization processes: (a) fast crystallization; (b) slow crystallization.

It is known that polymers with different degrees of crystallinity show different degrees of transparence. Figure 24 (a) is the HDPE sample that experienced a fast temperature change rate; it is more transparent, indicating a lower extent of crystallinity. Figure 24 (b) is the sample that experienced a slow temperature change rate; it is more translucent, indicating a higher degree of crystallinity. These results support the above argument that the amount of decrease in surface tension is related to the rate of temperature change and the extent of polymer crystallization.

4.4 Summary

The surface tension dependence of the crystalline polymer HDPE in supercritical N_2 on temperature and pressure was obtained experimentally and compared with that of the amorphous polymer PS in CO_2. At temperatures above the melting point, the trends of the surface tension change with temperature and pressure of HDPE are similar to those of PS, i.e., the surface tension decreases with increasing temperature and pressure. When crystallization of HDPE occurs, the surface tension decreases with decreasing temperature. During crystallization, polymer micro-crystals form and may act like nanoparticles in polymer melts, reducing the surface tension. It is found that the amount of decrease in surface tension is related with the temperature change rate, and hence the rate of crystallization; the surface tension decreases more with a slower temperature change rate, or a higher degree of crystallinity.

Chapter 5

Surface Tension of High Density Polyethylene-Clay Nanocomposites in Supercritical Nitrogen

5.1 Objectives

It has been proved that compared to pure HDPE foams, the addition of clay remarkably increased the cell density and reduced the cell size. That is, the addition of a small amount of clay, e.g., 1.0 and 3.0 wt%, produced a very high cell density of 10^{13} cells/cm^3 with an average cell size significantly smaller than 1 mm (i.e., close to nanocellular structure). These results suggest that the polymer cellular morphology was presumably affected by enhanced heterogeneous cell nucleation at the boundaries of the clay particles, polymer crystallinity, and rheological properties (Y. H. Lee, *et al.,* 2005). As we already know the importance of surface tension in the role of cell nucleation, the primary purpose of this work is to find the surface tension of HDPE-clay nanocomposites (HNC) under various temperatures and pressures. The results of HNC with different clay concentrations will be compared along with pure HDPE to find a trend and the minimum surface tension point.

An understanding of the degree of crystallinity for a polymer is important since crystallinity affects physical properties, such as storage modulus, permeability, density, and melting point. Thus, corresponding polymer crystallinity at different concentrations was measured by DSC to find a possible relationship with the surface tension. This study will have diverse impacts on the process optimizations of microcellular foaming process, which provides an explanation for the better foaming quality of HNC.

5.2 Experimental

5.2.1 Differential Scanning Calorimetry (DSC) Measurement: Crystallinity of HNC

Differential scanning calorimetry (DSC) was used to study the melting and crystallization of HNC as well as to determine the degree of crystallinity. DSC provides a rapid method for determining polymer crystallinity through the measurement of the enthalpy of fusion and its normalization to the enthalpy of fusion of 100 % crystalline polymer. Precision is typically a few percent. (B. Wunderlich, 1990) Since the previous thermal history of a polymer affects the measured degree of crystallinity, these samples were evaluated after being subjected to a "thermal treatment" designed to impart equivalent thermal history to all three samples. This thermal treatment consisted of heating at 20ºC/minute to 180 ºC, followed by controlled cooling at 30ºC/minute to 40ºC. Then the whole procedure was repeated and these second round results were used for the calculation of melting point, crystallization point and degree of cystallinity. (F.A. Quinn, Jr., 1958; B. Wunderlich, 1967; C.M.L. Atkinson, 1969; M.J. Richardson, 1972)

5.2.2 Surface Tension Measurement

The surface tension of 0.5%, 3%, 5% HNC in supercritical nitrogen were measured by ADSA-P at different temperatures from 130 to 160 °C in intervals of 10 C°, and three different pressures 500, 1000, and 1500 psi. Experiments at higher temperatures were performed as well, but obvious oxidation occurred at ~170°C, which was lower than pure HDPE (~ 200°C). The experimental setup was tested for its accuracy and reproducibility with a range of polymer-gas combinations, and the details of this setup and validation for

the surface tension measurement were described in a recent publication. (H. Park, 2006) Details about the technique (ADSA-P) and the calculations were described in Chapter 3, the experimental section. The surface tension value of HNC in supercritical nitrogen under various conditions was taken at its steady-state, when the change in surface tension was less than $0.0001 mJm^{-2}s^{-1}$ for 1h. Thus the values obtained are regarded as equilibrium surface tensions. For each equilibrium surface tension reported, errors were on the order of 0.01 mJm^{-2}.

5.3 Results and Discussion

5.3.1 Crystallinity of HNC

Figure 25 gives an example of the DSC results of 0.5% HNC. The peak point for the second round heating is around 131°C, which is considered as the melting point of the sample. Similarly, the peak point for the second round cooling is around 114°C, which is considered as the crystallization point of the sample. Using the software of Universal Analysis to integrate the second round peak area, the specific heat required for melting of the sample (ΔHm) is found to be ~181J/g. Dividing this value by the heat of fusion (293 J/g) for the pure crystalline phase of HDPE (ΔHm_0), we can obtain the crystallinity of this sample.
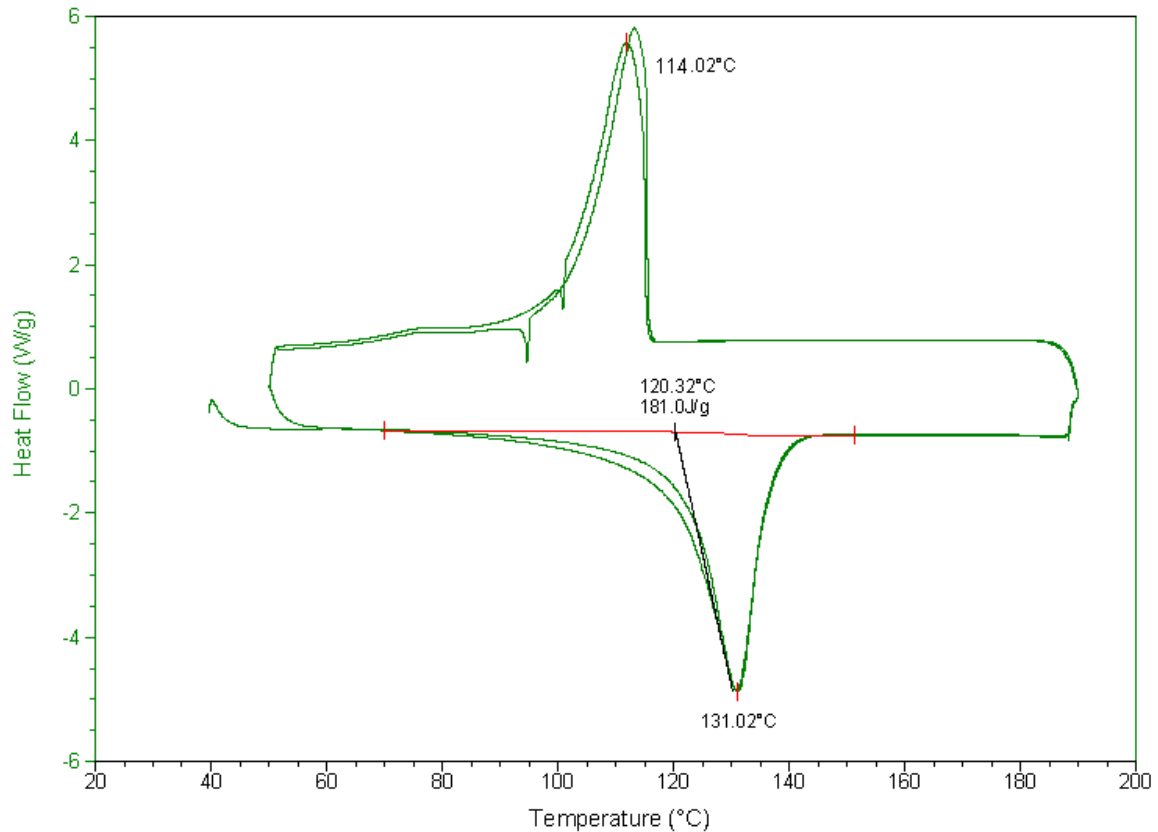
Fig. 25 DSC results for the 0.5% HNC at the heating rate of 20 ºC/min and cooling rate of 20 ºC/min. The procedure was: 1) Ramp 20 ºC/min to 190 ºC, 2) Equilibrate at 190 ºC, 3) Ramp 20 ºC/min to 50 ºC, 4) Isothermal for 2 minutes, 5) Ramp 20 ºC/min to 190 ºC, 6) Equilibrate at 190 ºC, 7) Ramp 20 ºC/min to 50 ºC

By repeating the same procedure for all the samples: pure HDPE, 3% HNC, and 5%HNC for 3 times, we are able to get the average melting point, crystallization point, and degree of crystallinity for each sample. The summarized results are shown in Table 3. Here, the melting point of pure HDPE ~130ºC is higher than the data obtained previously ~125 ºC. This is because of the thermal resistance between sample and sensor. The measured onset temperature increases linearly with increasing heating rate (the heating rate was increased from 5 ºC/min to 20 ºC/min).

Table 3 Melting and Crystallization Parameters of Used Samples Calculated from DSC

	Tm	Tc	Hm	Crystallnility
HDPE	132	109	168	0.57
HNC0.5%	132	113	177	0.60
HNC3%	133	115	186	0.63
HNC5%	132	115	176	0.60

The results in Table 3 illustrate that the crystallization temperature (Tc) and crystalline fraction of all nanocomposites increases compared with pure HDPE and then the crystalline fraction of nanocomposites decreases slightly as the clay content increases to a certain degree. A clear trend is found in Figure 26, with a maximum crystallinity shown at ~3%. The higher crystallization temperature suggests that faster nucleation occurred because of the nucleating role of clay. The larger crystallinity of all HNC than pure HDPE is caused by the addition of clay. Additionally, smaller crystalline fractions with the increase of clay concentration are due to the inability of the polymer chains to be fully incorporated into the growing crystalline lamella. In other words, the presence of the dispersed clay particles prevents large crystalline domains from forming by the spatial restrictions exerted on the polymer chains by a large number of clay particles. (Y. H. Lee *et al.,* 2005)
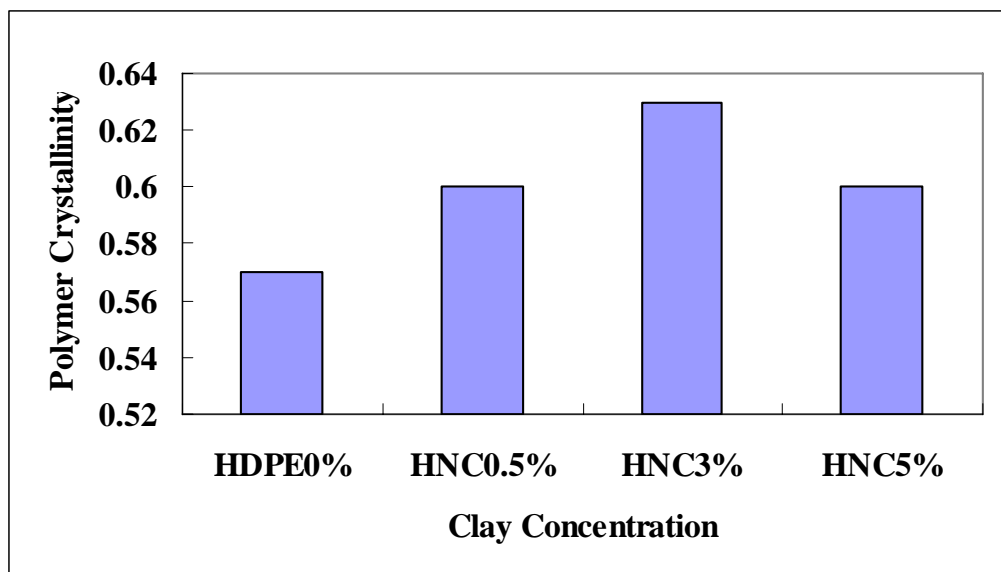
Fig. 26 Crystallinity fraction of HNC with different clay concentrations measured by DSC

5.3.2 Surface Tension of HDPE-Clay Nanocomposites with different clay concentration

The equilibrium surface tension value of the HNC melt in supercritical nitrogen was measured under various temperatures from 130 to 160 °C in intervals of 10 C°, and three different pressures 500, 1000, and 1500 psi. Figure 27 shows the equilibrium surface tension at each temperature and pressure.

For all four samples, it is apparent that at a given pressure, the surface tension decreases with increasing temperature; at a given temperature, the surface tension decreases with increasing pressure. The trend observed for the surface tension change with temperature is consistent with that of Wu, where a linear relationship between surface tension and temperature was proposed for polyethylene melts. (Wu, S., 1969) Linear regression models for the surface tension γ of HNC similar with Eq. (21) can be proposed against the experimental results.

$$\gamma \text{ (HNC } 0.5\%)=29.403-0.0489T-0.0016P \tag{26}$$

$$\gamma \text{ (HNC } 3\%)=25.328-0.0344T-0.0016P \tag{27}$$

$$\gamma \text{ (HNC } 5\%)=26.838-0.0382T-0.0018P \tag{28}$$

The trends of γ with T and P seem to be consistent with that of the surface tension of polystyrene (PS) in supercritical CO_2 (H. Park, 2007) and pure HDPE in supercritical N_2 discussed in Chapter 2 and Chapter 4.
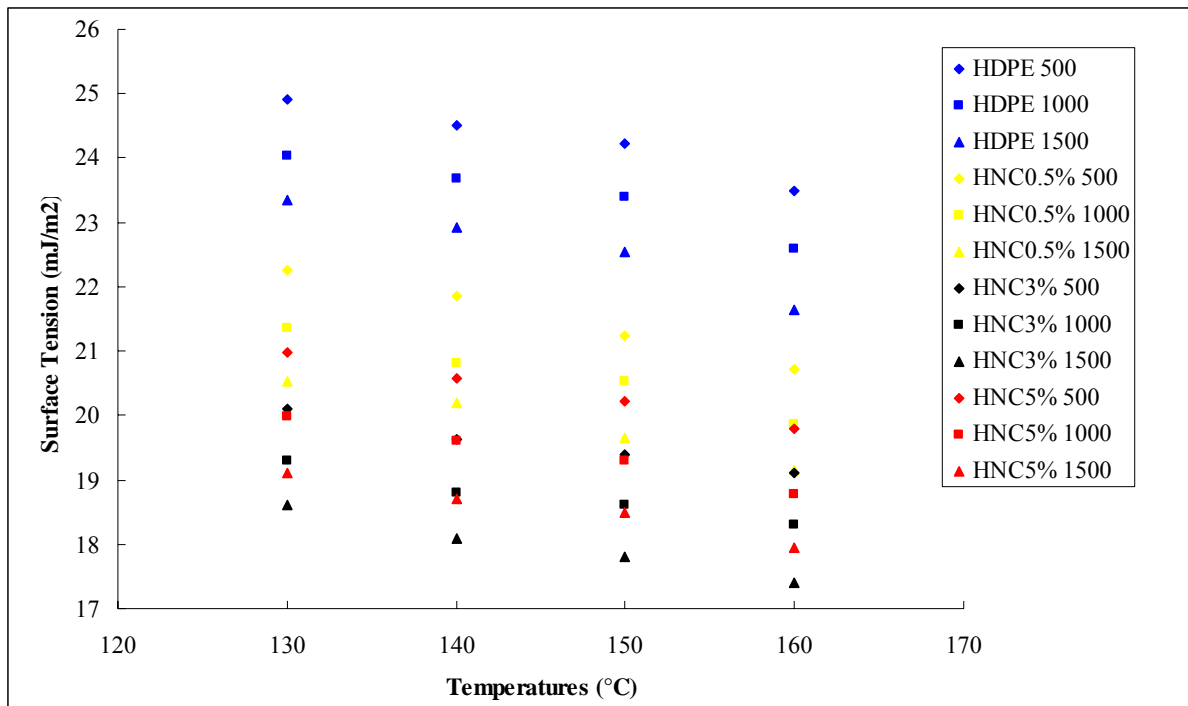
Fig. 27 The equilibrium surface tension of HDPE and HNC (0.5%, 3%, 5%) in N_2 at various temperatures (130, 140, 150, 160 ºC) and pressures (500, 1000, 1500 psi)

Figure 28 shows the surface tension of different samples as a function of clay concentration. Here we define the concentration in pure HDPE to be zero. It is clear that the surface tension for all the HNC samples is smaller than pure HDPE at a certain temperature and pressure. The surface tension first decreases with an increase in the amount of clay until a minimum value showed up at ~3%, and then increases back a little with further addition of clay. At 160°C, 1500psi, the surface tension of 3% HNC can be as low as ~17.3 mJ/m^2, which is around 20% lower than that of pure HDPE ~21.7 mJ/m^2.
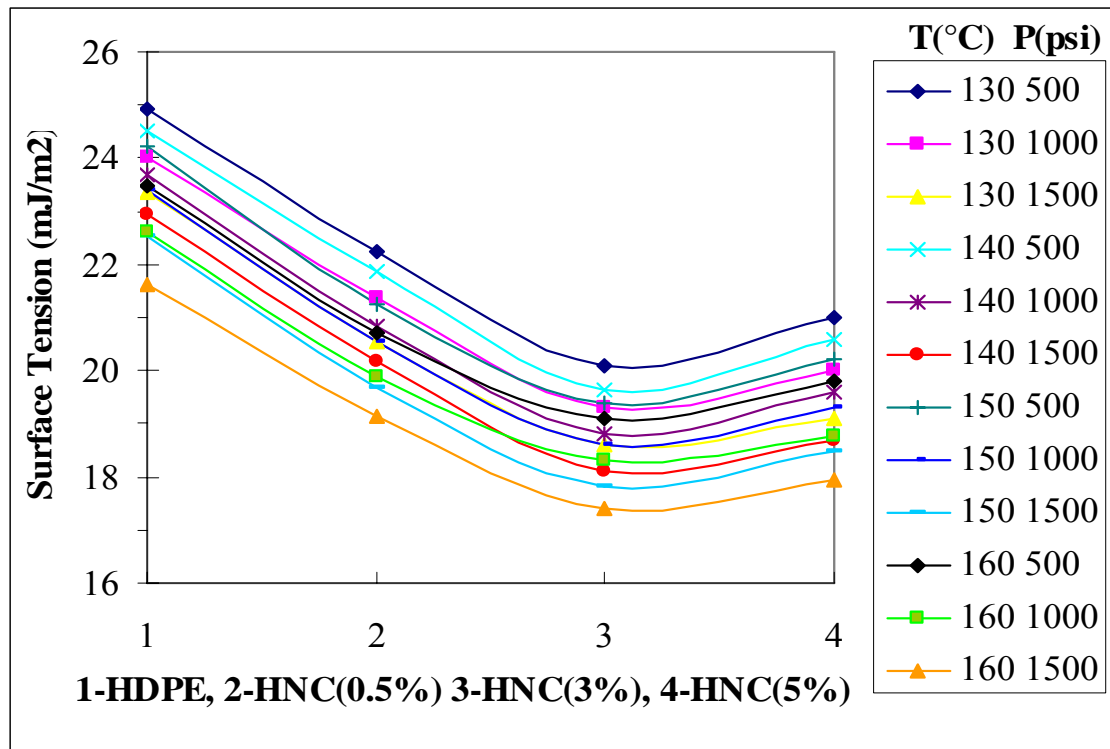
Fig. 28 The equilibrium surface tension of HDPE and HNC (0.5%, 3%, 5%) in N$_2$ as a function of clay concentration

5.3.3 The Correlation between Surface Tension and Crystallinity

For pure HDPE, we already found that during crystallization as the temperature decreases, surface tension decreases with the formation of crystals. Here, the lowest surface tension was found for 3% HNC, which has the highest crystallinity as well. Until now, we can not decide where those crystals are located. It is highly likely that these small, nano-sized crystals are formed in the polymer melt. It is also possible that some of these occur at the surface. Wu reported that for one polymer, the crystalline part should have a higher surface tension than the amorphous part. And by coming in contact with different interfaces, e.g, nitrogen, gold, during the crystallization process, the crystallinity of the surface would be different (Wu, S., 1982). We are not sure about the direct relationship between the surface tension and the degree of polymer crystallinity till date. But from the results and Wu's Concepts, it is quite possible that those crystals are located more in the bulk than on the surface, which change the interaction energy between polymer chains and in some way result in a reduced surface energy.

5.4 Summary

The results of HDPE-clay nanocomposites (HNC) with 0.5%, 3%, and 5% clay concentrations were measured and compared with pure HDPE. The dependence on temperature and pressure is the same for all samples, i.e., surface tension increases with decreasing temperature and pressure. At the same temperature and pressure, a minimum surface tension was found at 3% clay concentration HNC. The degree of crystallinity of HNC at different clay concentrations was measured with DSC. The crystallinity increases with the addition of clay and then decreases, with a maximum value also found at 3% clay concentration HNC. Further increase of clay concentration counteracts the polymer chains to be fully incorporated into the growing crystalline lamella, thus reducing the crystallinity.

Chapter 6

Original Contributions and Recommendations

6.1 Original Contributions

It has been found that the surface tension of amorphous polymers at temperatures below the melting point does not change significantly. But to date, the surface tension of crystalline polymers has not been measured at temperatures below the melting point. This thesis presents the surface tension of high density polyethylene and its nanoclay composites melts in supercritical nitrogen under various temperatures and pressures, using the Axisymmetric Drop Shape Analysis-Profile (ADSA-P) method.

The results of the crystalline polymer, HDPE in supercritical N_2 were compared with that of the amorphous polymer PS in CO_2. Surface tension dependence on temperature and pressure was obtained experimentally and related with the solubility of gas in the polymers. At temperatures above the melting point, the trends of the surface tension change with temperature and pressure of HDPE are similar to those of PS. i.e., the surface tension decreases with increasing temperature and pressure. When crystallization occurs, the surface tension decreases with decreasing temperature. During crystallization, polymer micro-crystals form and may act like nanoparticles in polymer melts, reducing the surface tension. It is found that the amount of decrease in surface tension is related with the rate of temperature change, and hence the rate of crystallization; the surface tension decreases more with a slower temperature change rate, or a higher degree of crystallinity. This work has been summarized as a paper called "Surface tension of high density polyethylene (HDPE) in

supercritical nitrogen: Effect of polymer crystallization" and published on Colloids and Surfaces A.

The results of HDPE-clay nanocomposites (HNC) with different clay concentrations were measured and compared with pure HDPE. The dependence on temperature and pressure is the same for all samples, i.e., surface tension increases with decreasing temperature and pressure. At the same temperature and pressure, a minimum surface tension was found at 3% clay concentration HNC. The degree of crystallinity of HNC at different clay concentrations were measured with DSC. The crystallinity increases with the addition of clay and a maximum crystallinity was also found at 3% clay concentration HNC. Further increase of clay concentration counteracts the polymer chains to be fully incorporated into the growing crystalline lamella, thus reducing the crystallinity. To compare the surface tension and polymer crystallinity, considering the crystallization process of HDPE and the experiments on different clay concentrations of HNC, it is presumable that the surface energy gets lower when the internal crystallinity gets higher. This study will have diverse impacts on the process optimizations of microcellular foaming process, which gives an explanation for the better foaming quality of HNC.

6.2 Recommendations

This thesis focuses on the surface tension measurement of high density polyethylene and its nanoclay composites in supercritical nitrogen. Experimental results have showed the decrease of surface tension with the formation of crystals and the addition of clay. The author suggests further experiments on finding where the crystals and clays are located (more on the surface or more in the bulk).

In the past decade, the use of nanometer-sized layered silicate particles had garnered a great deal of attention. Adding a small amount of nanoparticles can dramatically improve a wide variety of properties of the polymer matrix, offering unique properties. Recently, porous silica was obtained with nonionic surfactants and block copolymers as templates (Éric Prouzet, *et al.*, 2005). By compositing polymers with these porous particles, we may expect a much different behavior in the foaming process.

Polymer carbon nanocomposites have excellent mechanical features (high degrees of strength and toughness) and conductivity (heat and electricity) as well. A lot of products have been used for aerospace, automobiles, electronics, sports, and leisure. Fundamental studies of the surface behavior of these products would help to improve the quality and save the cost in the foaming industry.

Besides high density polyethylene, more experimental measurements on other polymers can be performed, e.g., low density polyethylene. To compare the results, we can further understand the relationship between polymer density, crystallinity and surface tension. Copolymers and other supercritical fluids can be tried in the future experiments.

Other parameters such as viscosity, solubility, molecular weight, molecular weight

distributions also have an impact on the foaming quality. More surface modifications in these areas are needed together with some mechanical tests.

Since the surface properties of materials are very important, the expertise gained from this research could be applied to lots of fields such as food engineering, pharmaceutical industry, polymer synthesis, foaming and coating.

References

Adamson, A. W. and Gast, A. P., Physical Chemistry of Surfaces, John Wiley & Sons, Inc., New York, 1997

Alexopoulos, A. H., Puig, J. E., Franess E. J. *J. Colloid Interface Sci.* 1989, 128, 26-34

Anastasiadis, S. H., Chen, J. K., Koberstein, J.T., Sohn, J. E. And Emerson, *J. A. Polym. Eng. Sci.* 1986, 26, 1410-1418

B.M. Epelbaum, M. Bickermann and A. Winnacker *Journal of Crystal Growth* 275, Issues 1-2, 2005, e479-e484

B. Wunderlich, Thermal Analysis, Academic Press, 1990, pp. 417-431

B. Wunderlich and C.M. Cormier, *J. Polymer Sci.,* Part A-2, 1967, 987

Cahn, J. W. and Hilliard J. E., *J. Chem. Phys.* 1959, 31, 688-699

Cheng, P.; Li, D.; Boruvka, L.; Rotenberg, Y.; Newmann, A. W. *Colloids Surf.* 1990, 43, 151-167

Cheng, P.; Neumann, A. W. *Colloids Surf.* 1992, 62, 297-305

C.M.L. Atkinson and M.J. Richardson, *Trans. Faraday Soc.,* 1969, 65, 1764

del Rio, O. I.; Neumann, A. W. *J. Colloid Interface Sci.* 1997, 196, 136-147

Demarquette, N. R.; Kamal, M. R. *Polym. Eng. Sci.* 1994, 34 (24),1823-1833

É. Prouzet, C. Boissière, *C. R. Chimie* 2005, 579–596

F. A. Quinn, Jr., and L. Mandelkern, *J. Am. Chem. Soc.,* 1958, 80, 3178

F. Bashforth, J. C. Adams, An Attempt to Test the Theory of Capillary Action, Cambridge University Press and Deighton Bell & Co., Cambridge, 1883

Giannelis, E.P. *Adv. Mater.,* 8(1): 29. 1996

Goel, S. K. and Beckman, E., *J. Polym. Eng.* Sci., 1994, 34, 1137-1147

Hess, M., *Macromol.* 2004, 214, 361-379

J. Campbell, *Journal of Physics D* 1970, 3, 1499-1504

Jürgen, E.K. Schawe *Thermochimica Acta* 2007 461 145–152

Krishnamoorti, E., Vaia, R.A. and Giannelis, E. P. *Chem. Mater.*, 1996, 8(8): 1718

Kojima, Y., Usuki, A., Kawasumi, M., Okada, A., Fukushima, Y., Kurauchi, T. and Kamigaito, O. *J. Mater. Res.,* 1993, 8(5): 1185

Lahooti, S.; Rio, O. I.; Cheng, P.; Neumann, A. W. *Applied Surface Thermodynamics*; Neumann, A. W., Spelt, J. K., Eds.; Marcel Dekker: New York, 1996

Lau, W. W. Y., Burns, C. M. *J. Colloid Interface Sci.* 1973, 45, 295-302

Lee, M., Park, C. B. and Tzoganakis, *C. Polym. Eng.Sci.* 1999, 9, 99-109

Lee, Y. H., Park, C.B., Sain, M., Kontopoulou, M., and Zheng, W.G., *Journal of Applied Polymer Science*, 2007 105 1993-1999

Li, G., Li, H., Wang, J., Park, C. B. *Cell Polym.* 2006, 25, 237

Li, G., Wang, J., Park, C. B., Moulinie, P., Simha, R. *Annu Tech Conf Soc Plast Eng.* 2004, 62, 2566

Li, H.; Lee, L. J.; Tomasko, D. L. *Ind. Eng. Chem. Res*. 2004, 43, 409

Morita, A. T.; Carastan, D. J.; Demarquette, N. R. *Colloid Polym. Sci.* 2002, 280, 857

Myers D. *Surfaces, Interfaces, and Colloids: Principles and Applications*; VCH Publishers: New York, 1991

M.J. Richardson, *J. Polymer Sci. C*, 1972, 251

Nishioka, K.; Kusaka *J. Chem. Phys.* 1992, 96 (7), 5370-5376

Park, H. "Surface Tension Measurement of Polystyrenes in Supercritical Fluids" 2007, PhD thesis, University of Waterloo

Park,H., C. B. Park, C. Tzoganakis, P. Chen *Ind. Eng. Chem.* 2007, 46, 3849-3851

Park, H.; Park, C. B.; Tzoganakis, C.; Tan, K. H.; Chen, P. *Ind. Eng. Chem. Res.* 2006, 45, 1650-1658

Park, H., Thompson, R.B., Lanson, N., Tzoganakis, C., Park, C.B. and Chen, P. *J. Phys. Chem. B* 2007, 111, 3859-3868

Pijpers, T.F.J., Mathot, V.B.F., Goderis, B., Scherrenberger, R.L., and vander Vegte, E.W. *Macromolecules* 2002 33 3601.

Quach, A., Simha, R., *Journal of Applied Physics* 1971, 42, 4592-4606

Roe, R.J.; Bacchetta, V. L.; Wong, P. M. G. *J. Phys. Chem.* 1967, 71, 4190

Royer, J. R., Gay, Y. J., Desimone, J. M., Khan S. A. *Journal of Polymer Science B* 2000, 38, 3168-31380

R. A. L. Jones and R. W. Richards, Polymers at Surfaces and Interfaces, Cambridge University Press, New York 1999

R. B. Thompson, J. R. MacDonald and P. Chen, *Physical Review E* 2008, 78, 030801(R)

Sanchez, I. C. and Lacombe, R. H. *J. Phy. Chem.* 1976, 80, 2352-2362

Sanchez, I. C. and Lacombe, R. H. *Macromolecules* 1978, 11, 1145-1156

Seeler, K.A. and Kumar, V., *ASME, Cellu Polym*, 1992, 38, 93

Shenoy, S. L.; Fujiwara, T.; Wynne, K. J *Macromol.* 2003, 36, 3380

Simha, R., Somcynsky, T. *Macromolecules* 1969, 2, 342

Song, B. and Spinger, J. *J. Colloid Interface Sci.* 1996, 184, 77-91

Susnar, S. S.; Hamza, H. A.; Newmann, A. W. *Colloids Surf.* 1994, 89, 169-180

Tomasko, D. L., Li, H, Liu, D., Han, X., Wingert, M. J., Lee, L. J. and Koelling, K. W. *Ind. Eng. Chem.* Res. 2003, 42, 6431-6456

Utracki, L. A. *Journal of Polymer Science B* 2007, 45, 270-285

Wang, K. H., Chung, I. J., Jang, M.C., Keum, J. K. and Song, H. H. *Macromolecules,* 2002, 35(14): 5529

Wang, K.H., Xu, M., Choi, Y.S. and Chung, I.J. *Polymer Bulletin,* 2001, 46: 499

Wu, S. *Journal of Colloid and Interface Science,* 1969, 31, 2

Wu, *S. J. Phys.Chem.* 1970, 74, 632

Wu, S. *Polymer Interface and Adhesion*; Marcel Dekker: New York, 1982
Wunderlich, *B. J. Phys.Chem.*1958 29 6

Wunderlich, *B. Macromolecular Physics* vol. 1, Academic Press, New York, 1973

Wunderlich, *B. Macromolecular Physics* vol. 3, Academic Press, New York, 1980

Wunderlich, B. and Czornyj, G. *Macromolecules,* 1977, 10(5): 906

Xue, A.; Tzoganakis, C.; Chen, P. *Polym. Eng. Sci.* 2004, 44, 18

Y. H. Lee, C. B. Park, K. H. Wang, and M. H. Lee, *J. Cellu Plast* 2005, 41

Y. H. Lee, Chul B. Park, M. Sain, M. Kontopoulou, Wenge Zheng *Wiley InterScience* 2007, 1

Yoshiyuki Sato, Tadao Takikawa, Atsushi Sorakubo, Shigeki Takishima, Hirokatsu Masuoka, and Mitsuhiro Imaizumi *Ind. Eng. Chem.* Res. 2000, 39, 4813-4819

Yu.A. Shlyapnikov, I.A. Serenkova, Die Angewandte Makromolekuhre Chemie 1983, 114, I -I 1 (I 836)

Zachmann, H.G. Fortschr. *Hochpolym. Forsch*. 1964 3 581

Zoller, P., Bolli, P., Pahud V., Ackermann H., *Rev. Sci. Instrum.* 1976, 47, 948-952

Appendix A

Self-Consistent Field Theory

To understand the surface tension and its dependence on temperature and pressure, experimentally determined surface tensions can be compared to surface tensions calculated using self-consistent field theory (SCFT). SCFT is an equilibrium statistical mechanical approach for determining structures in polymeric systems. It is based on a free energy functional, which is to be minimized in order to find the lowest free energy morphology. The procedure for deriving such functionals has been explained in depth in a number of reviews [1-5]. For the supercritical carbon dioxide-polystyrene system, an appropriate free energy functional has been derived in the canonical ensemble in Ref. [6]

In order to find the free energy of the system, a number of input parameters are needed. In the canonical ensemble, one needs the volume V as well as ϕ_s, ϕ_p, and ϕ_h representing the overall volume fractions of solvent molecules, polymer segments and "holes", respectively. One also needs the degree of polymerization N, which is based on a segment volume $1/\rho_0$. Since SCFT is a coarse-grained theory, a single segment may include many chemical monomers. In order to be consistent with the Sanchez-Lacombe equation of state [7, 8] being used experimentally to extract the surface tension in the supercritical carbon dioxide-polystyrene system, a Sanchez-Lacombe equation of state was used to model pressure in the SCFT. This approach was introduced by Hong and Noolandi [9] for SCFT and consists of treating a compressible system as an incompressible system together with vacancies, that is, holes. Higher pressure systems have fewer holes whereas lower pressure systems have more. The Sanchez-Lacombe equation of state thus relates the density to

pressure for systems whose variable density is modeled in terms of holes. The volume fractions ϕ_s, ϕ_p, and ϕ_h, are therefore not all independent, rather $\phi_s + \phi_p + \phi_h = 1$. Other approaches for treating compressibility within SCFT are possible, in particular Binder *et al.* have studied solvent-polymer systems using a virial expansion to get an equation of state [10]. Flory-Huggins parameters are also required inputs; these are usually defined in terms of dissimilar constituents such as χ_{ps}, χ_{pk} and χ_{sk}. In Ref. [6] however, since the holes are fictitious, it was more meaningful to choose the three independent parameters as χ_{ps}, χ_{pp} and χ_{ss}. They were defined from first principles as

$$\chi_{ij} = \frac{\rho_0}{k_B T} \int d\mathbf{r} V_{ij}(|\mathbf{r}|) \tag{1}$$

where $V_{ij}(|\mathrm{r}|)$ was two-body potential between species i and j with i, $j=p$, s or h [9], and k_B is Boltzmann's constant. Since the potential between holes and anything else should be zero, all χ terms in the free energy involving h would vanish. The interpretation of these parameters was then no longer as the dimensionless change in energy upon exchange of segments between pure components, although the use of the term Flory-Huggins parameter would be maintained; they still arose as the first order in a gradient expansion of the potentials. Usually, the products χN are taken as the segregation parameters instead of just the parameters χ, and this was done in Ref. [6]. Lastly, one requires the ratio of the volume of a solvent molecule to a polymer molecule, which in [6] was given by α. The free energy functional was varied with respect to position dependent volume fraction functions and chemical potential functions to yield a set of equations that was solved numerically and self-consistently.

The free energy functional can be used to calculate the free energy for the whole system, as well as the free energies for two homogeneous systems equivalent to the bulk regions of the

original system. Subtracting the homogenous free energies from the total free energy gives the excess free energy of the interface which, when divided by the surface area, is the surface tension. Details of the procedures can be found in Ref. [6].

To facilitate analysis of results, the surface tension can be broken up into thermodynamic components. The components chosen in Ref. [6] were the internal energy contributions to the free energy between polymer segments and solvent, solvent and solvent, and polymer and polymer, the translational entropy contribution to the free energy of the polymer, the configurational entropy of the polymer, the translational entropy of the solvent and the translational entropy of the holes. The configurational entropy accounts for the different conformations a polymer can take, whereas the translational entropy of the polymer accounts for the remaining positional degrees of freedom of the center of mass of a molecule. These components can be converted into excess free energy components by subtracting off the corresponding bulk free energy components of the homogenous phases on either side of the interface in exactly the same way as for the total free energy. Then by dividing by the interfacial area, these can be converted into components of the surface tension, just as the total excess free energy was expressed as a surface tension. These internal energy and entropic contributions to the surface tension were used in Ref. [6] to explain the trends observed experimentally in the supercritical carbon dioxide-polystyrene system, albeit only qualitatively.

The SCFT calculations were performed to find a dimensionless surface tension as a function of temperature at two different pressures. For the high pressure run, no holes were included and the overall volume fractions were taken as ϕ_p=0.65 and ϕ_S=0.35 for the

polymer and solvent, respectively. This corresponds to an incompressible fluid, and thus is the highest pressure case possible. This was compared against a lower pressure run with ϕ_p =0.60 and ϕ_S=0.30, or in other words, with 10 percent holes by volume. In both cases and at all temperatures, the system size (considering one dimension) was $L=12.0R_g$, where R_g is the unperturbed radius of gyration of a polymer. The ratio α of the volume of a solvent molecule to that of a polymer molecule was taken to be 0.1 for both pressure runs. This was not particularly realistic, as this ratio for the supercritical carbon dioxide-polystyrene system should be a much smaller number. Too great a size disparity between the different molecular species would however cause numerical difficulties. This resulted from the extremely high translational entropy of many, very small solvent molecules. This strongly favored mixing, and made it difficult to establish an interface unless the Flory-Huggins parameters were turned up extremely high. This in turn made it difficult to achieve numerical accuracy in the calculations. Rather, a qualitative approach was taken, making sure that trends observed experimentally were nonetheless still observed in the calculations despite a large value for α.

Given the qualitative philosophy, it sufficed to choose Flory-Huggins values that mapped the model system qualitatively onto the experimental structure. A relationship between χ (or in this case, χN) and temperature T that is commonly used is [11, 12]:

$$\chi N = \frac{A}{T} \ + \ B \tag{26}$$

where A and B are constants. In Ref. [6] there were three different such parameters, namely $\chi_{ps}N$, $\chi_{ss}N$ and $\chi_{pp}N$, so there were three sets of constants, $A_{ps}, B_{ps}, A_{ss}, B_{ss}$ and A_{pp}, B_{pp}. The constants B_{ps}, B_{ss} and B_{pp} were all set to zero for simplicity, as was A_{pp}. From Eq. (26), A_{pp} =0

can only be satisfied for arbitrary T if $\chi_{pp}N = 0$, always. The remaining parameters were chosen as $A_{ps}=100$ and $A_{ss}=150$. The temperature T was ranged, in arbitrary units, from 2.0 to 2.5 giving

$$2.0 < T < 2.5$$

$$50 > \chi_{ps}N > 40$$

$$75 > \chi_{ss}N > 60.$$

These values produced reasonable interfacial structures, as shown in Ref. [6]. To assign specific units to the temperature such as Kelvin or degrees centigrade, the parameters A should be specified in the desired units. The present values were chosen so as to reproduce an appropriate interface while at the same time allowing for numerically accurate calculations.

Temperature dependence
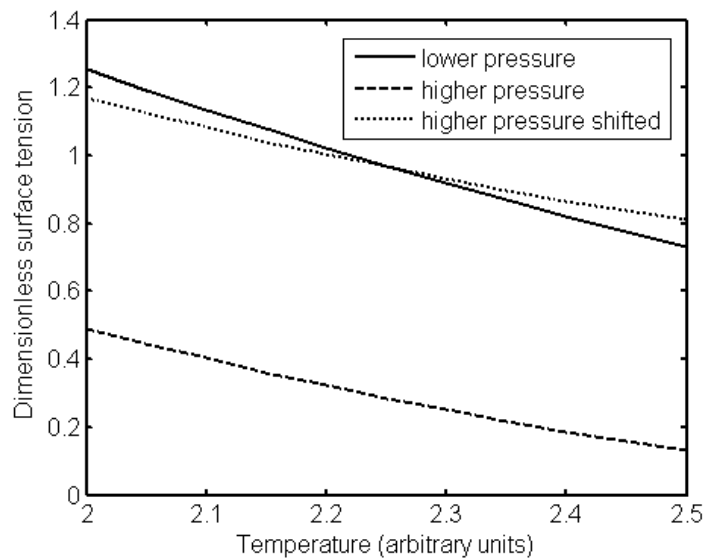
Fig. 1 Dimensionless surface tension as a function of temperature for two different pressures. The lower pressure run is the solid curve while the higher pressure run is the dashed curve. The higher pressure run is also plotted a second time by a dotted curve where it is shifted upwards to more easily compare the slopes of the two runs.

Figure 1 shows the dimensionless surface tension results from Ref. [6] as a function of temperature at two different pressures.

The results can explain the three main trends mentioned in section 2.4. The temperature dependence of the model system can be seen to follow the trends of experiment and the empirical equation (12) at both pressures in that surface tension decreases with increasing temperature. In Figure 2 the components of the surface tension are plotted. The two main components that can be seen to be contributing to the decrease of surface tension with temperature are the internal energy contribution to the surface tension (open circles on solid curve) and the polymer configurational entropy contribution to the surface tension (crossed dotted curve). The translational entropy of the holes contributes negligibly. The largest contribution is from the internal energy.

(a)   (b)

Fig. 2 Components of the surface tension for (a) the lower pressure run and (b) the higher pressure run. Different contributions to the surface tension are shown in the legends.

This contribution can in turn be split into the polymer-solvent, solvent-solvent, and polymer-polymer components of the internal energy contribution to the surface tension, as shown in Figure 3. In that figure, the component that is clearly responsible for the overall drop of the total internal energy contribution is the polymer-solvent component; it is the only component with a slope in the correct direction. Translating this conclusion into polymer-solvent processes, one would concentrate on modifying the molecular interaction between the polymer and its solvent when making use of such temperature dependence of surface tension. Under this situation, modifications of polymer or solvent molecular properties alone could be less effective at reducing surface tension with an elevated temperature.

(a)   (b)

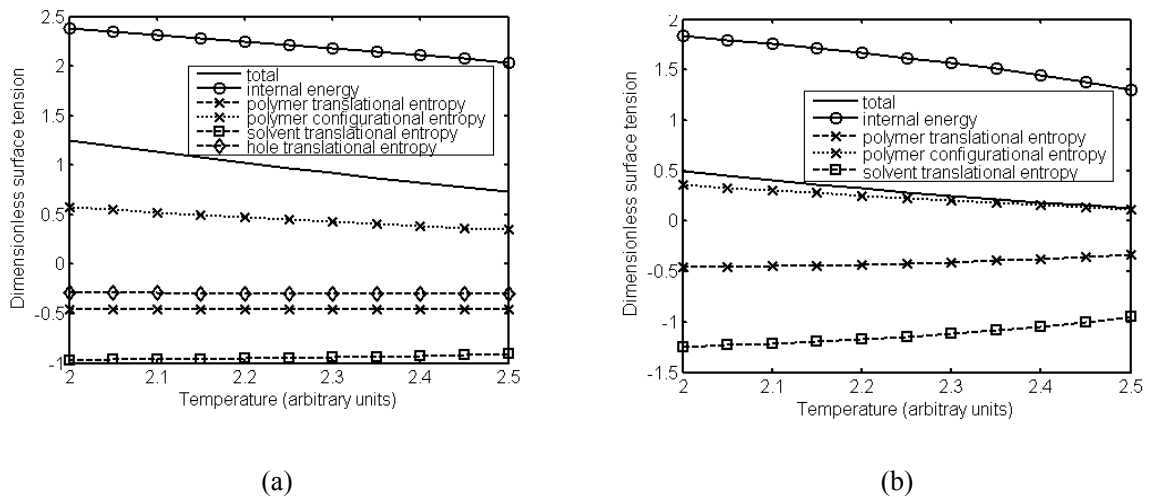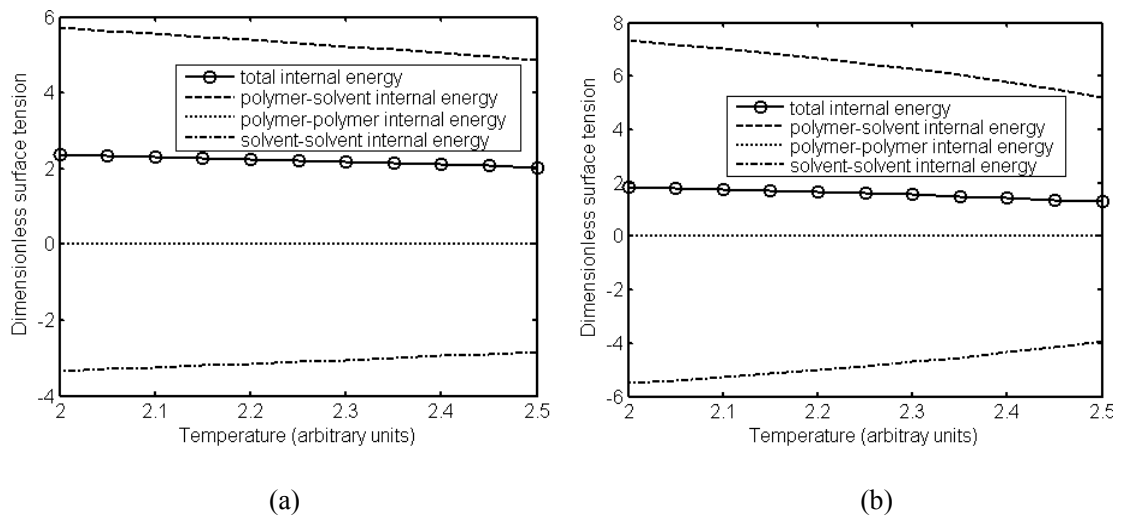Fig. 3 Sub-components of the internal energy contribution to the surface tension for the (a) lower pressure run and (b) the higher pressure run. Different contributions to the surface tension are shown in the legends.

That the polymer-solvent internal energy contribution is responsible for the drop in surface tension makes perfect sense, in that the free energy of the system can be split into an internal

energy part and an entropic part, the two parts having different signs, that is, they oppose each other. The entropic contributions promote mixing whereas the internal energy favors segregation. As the temperature is increased, the $\chi_{ps}N$ parameter decreases, reducing the segregation between polymer and solvent segments. This means the entropy becomes a larger relative portion of the free energy, more mixing takes place and the interface becomes more diffuse; this in turn means there would be a lower surface tension. This is a well known and understood effect which was correctly reproduced in the model system of Ref. [6].

Pressure dependence

In Figure 1 it can be seen that the surface tension versus temperature curve drops to lower surface tension for a higher pressure. This is again in agreement with the experimental findings and empirical equation (12). The components of the surface tension that drop are the internal energy, the configurational entropy of the polymer and the translational entropy of the solvent; this can be seen from Figure 2 by comparing panels (a) and (b). Again, the largest single factor causing this drop is the internal energy contribution. In Figure 3, however, it is seen that for the pressure induced surface tension drop, the responsible sub-component is not the polymer-solvent internal energy as for the temperature case, but rather the solvent-solvent sub-component. Translating this conclusion into industrial polymer-solvent processes, one could simply focus on modifying the molecular self-interaction among solvent molecules when making use of such pressure dependence of surface tension.

The above conclusion can be understood in terms of a reduction of dilution by the holes. At higher pressure, there are fewer holes present. Since $\chi_{ss}N$ was chosen to be positive, solvent molecules prefer to be in an environment of holes rather than in an environment of other

solvent molecules; in the former situation the unfavorable solvent-solvent contact energy is diluted by the holes. With the removal of holes at higher pressure, this dilution is reduced, the solvent-solvent contact energy goes up, and so does the free energy. This effect takes place predominantly in the bulk solvent side of the interface where the majority of solvent molecules can be found. This means the bulk free energy is increased. This increased quantity is subtracted off the total free energy to find the surface tension, therefore the surface tension would drop.

This last point may be understood in terms of density. The removal of holes is the same as an increase in density in the region where the holes are being removed. Thus the surface tension drops when the solvent phase increases in density to be more similar to the density on the polymer side of the interface. Thus one can say the drop in surface tension with increasing pressure is due to a reduction of the density difference between two sides of the interface.

The above analysis of pressure dependence required a χ_{ss} that was positive, and so it is appropriate here to discuss what might be the case if χ_{ss} were negative. This is important since from the first principles definition of χ_{ss} given in Eq. (1) one would expect that χ_{ss} would normally be less than zero, that is, the solvent molecules would have some slight attraction. For more realistic choices of α, the translational entropy of the solvent would not be negligible. Therefore instead of holes diluting the solvent phase for energetic reasons, the holes would dilute the phase for entropic reasons. The explanation would remain the same for the pressure dependence beyond this, and the density difference interpretation would still hold. As α is increased, the translational entropy of the solvent will become less important, and to maintain the interface structure, χ_{ss} must be made less negative. For a very large α, such

as is being used here, χ_{ss} must become positive to draw the hole molecules into the solvent phase to reproduce the experimental configuration. At this point, χ_{ss} must be viewed entirely as a phenomenological parameter.

Change in temperature dependence with pressure

In addition to an overall drop in surface tension upon increasing pressure, the temperature dependence of the surface tension is less pronounced at high pressures than at lower pressures. This is seen in Figure 1 where the dotted curve is a repetition of the high pressure curve (dashed) shifted upwards to lie on top of the lower pressure curve (solid). One can clearly see the shallower slope with temperature of the high pressure results. This is again in agreement with the experimental findings and the empirical equation (12).

From Figure 2, one can compute linear slopes for all the components of the surface tensions in order to find which components are responsible for this reduction in steepness. It was found that the translational entropy components of the polymer, solvent and holes all contributed to the overall reduction in steepness. The hole contribution was negligible compared to the other two and could safely be ignored. Thus it was the polymer and solvent translational entropy contributions to the surface tensions that caused the shallowness of the high pressure results.

This is explained in terms of the presence or absence of holes. The presence of holes can only affect the system in two ways: through energy dilution as discussed in the pressure dependence subsection, or through adding translational entropy. The latter was said to be insignificant, and so we are left with energy dilution alone. At low pressures, the solvent-solvent contacts are diluted by the holes, reducing the system free energy. At high pressures, solvent-solvent contacts cannot be reduced by holes anymore, so the only

89

possibility for reducing these contacts is for the solvent to be near polymer segments. This can induce increased mixing, and thus increase translational entropy of both the solvent and the polymer. This increased mixing partially counteracts the internal energy segregation effect that is a function of temperature. Thus the surface tension profile with temperature is flatter at higher pressures than at lower pressures where this polymer-solvent mixing is unnecessary due to the presence of the holes. In other words, when the solvent is at higher density, there is a greater mixing effect that counteracts the formation of an interface due to a solvent-solvent internal energy reduction upon absorbing solvent into the polymer phase.

For small α values and negative χ_{ss} parameters, the same mechanism is expected to function, except that translational entropy would force the holes into the solvent phase rather than energetic considerations, along the lines explained in the pressure dependence section.

References

[1] Wu, S. Journal of Colloid and Interface Science, 1969, 31, 2

[2] Matsen M. W. In Soft Matter Volume 1; Eds. Gompper, G; Schick, M.; Wiley-VCH :Weinheim 2005, 87-178

[3] Matsen, M. W. J. Phys. Condens. Matter 2002, 14, R21-R47

[4] Fredrickson, G. H.; Ganesan, V.; Drolet, F. Macromolecules 2002, 35, 16-39

[5] Schmid, F. J. Phys. Condens. Matter 1998, 10, 8105-8138

[6] H. Park, R. B. Thompson, N. Lanson, C. Tzoganakis, C. B. Park, and P. Chen J. Phys. Chem. B 2007, 111, 3859-3868

[7] Sanchez, I. C. and Lacombe, R. H. J. Phy. Chem. 1976, 80, 2352-2362

[8] Sanchez, I. C. and LaFcombe, R. H. Macromolecules 1978, 11, 1145-1156

[9] Hong , K. M.; Noolandi, J. Macromolecules 1981, 14, 1229-1234

[10] Binder, K.; Müller, M.; Virnau, P.; MacDowell, L.G. Adv. Polym. Sci. 2005, 173, 1-110

[11] Mai , S.-M.; Fairclough, J. P. A.; Terrill, N. J.; Turner, S. C.; Hamley, I. W.; Matsen, M. W.; Ryan, A. J.; Booth, C. Macromolecules 1998, 31, 8110-8116

[12] Mai, S. -M.; Mingvanish W.; Turner S. C.; Chaibundit, C.; J. P. A.; Heatley, F.; Matsen, M. W.; Ryan, A. J.; Booth C. Macromolecules 2000, 33, 5124-5130

Appendix B

Density Determination Data

Density difference data between HDPE and nitrogen at various temperatures and pressures

in units of g/cm³

Temperature (°C)	PRESSURE (psi)			
	500	1000	1500	2000
100	0.778	0.749	0.725	0.697
110	0.774	0.746	0.722	0.695
120	0.770	0.743	0.719	0.693
130	0.766	0.74	0.716	0.690
140	0.762	0.737	0.713	0.688
150	0.758	0.734	0.710	0.686
160	0.754	0.731	0.707	0.684
170	0.750	0.727	0.704	0.681
180	0.745	0.724	0.701	0.678
190	0.741	0.720	0.698	0.676
200	0.736	0.715	0.696	0.673

Appendix C

Example of Rough Data Obtained by ADSA-P

File Name	Surface Tension	Surface Area	Volume	Radius of Curvature
	mJ/m^2	(cm^2)	(cc)	(cm)
1	21.5379	0.1888	0.0085	0.1067
2	21.5029	0.1892	0.0085	0.1067
3	21.5411	0.1889	0.0085	0.1067
4	21.6005	0.1891	0.0085	0.1068
5	21.5526	0.1891	0.0085	0.1068
6	21.5254	0.1888	0.0085	0.1067
7	21.4509	0.1885	0.0085	0.1066
8	21.5258	0.1888	0.0085	0.1067
9	21.6386	0.1893	0.0086	0.1069
10	21.4544	0.1885	0.0085	0.1066
11	21.5036	0.1888	0.0085	0.1067
12	21.5623	0.1891	0.0085	0.1068
13	21.5719	0.1888	0.0085	0.1067
14	21.5728	0.1888	0.0085	0.1068
15	21.4007	0.1882	0.0085	0.1065
16	21.5782	0.1891	0.0085	0.1068
17	21.5328	0.1889	0.0085	0.1067
18	21.5114	0.1886	0.0085	0.1067
19	21.4713	0.1886	0.0085	0.1066
20	21.5099	0.1886	0.0085	0.1067
21	21.4891	0.1886	0.0085	0.1067
22	21.5255	0.1889	0.0085	0.1067
23	21.4155	0.1883	0.0085	0.1065
24	21.5037	0.1888	0.0085	0.1067
25	21.5287	0.1886	0.0085	0.1067
26	21.5586	0.1886	0.0085	0.1068
27	21.5581	0.1887	0.0085	0.1067
28	21.5352	0.1888	0.0085	0.1067
29	21.5932	0.1889	0.0085	0.1068
30	21.5521	0.1890	0.0085	0.1067
31	21.5425	0.1888	0.0085	0.1067
32	21.5669	0.1889	0.0085	0.1068
33	21.4893	0.1885	0.0085	0.1067
34	21.4558	0.1883	0.0085	0.1066

File Name	Surface Tension	Surface Area	Volume	Radius of Curvature
35	21.5330	0.1887	0.0085	0.1067
36	21.5644	0.1889	0.0085	0.1067
37	21.4390	0.1885	0.0085	0.1066
38	21.6153	0.1890	0.0085	0.1069
39	21.5868	0.1888	0.0085	0.1068
40	21.4569	0.1882	0.0085	0.1066
41	21.5201	0.1886	0.0085	0.1067
42	21.4467	0.1883	0.0085	0.1066
43	21.4093	0.1883	0.0085	0.1066
44	21.3871	0.1883	0.0085	0.1066
45	21.5343	0.1891	0.0085	0.1067
46	21.6015	0.1890	0.0085	0.1068
47	21.4473	0.1882	0.0085	0.1066
48	21.5213	0.1888	0.0085	0.1067
49	21.5620	0.1885	0.0085	0.1067
50	21.6082	0.1890	0.0085	0.1068
51	21.5072	0.1882	0.0085	0.1066
52	21.5352	0.1887	0.0085	0.1067
53	21.5399	0.1887	0.0085	0.1067
54	21.5238	0.1886	0.0085	0.1067
55	21.5786	0.1887	0.0085	0.1068
56	21.4896	0.1885	0.0085	0.1067
57	21.5516	0.1888	0.0085	0.1067
58	21.6035	0.1890	0.0085	0.1068
59	21.5695	0.1888	0.0085	0.1068
60	21.4779	0.1886	0.0085	0.1067